RAI Volume 3, Chapter 2.2.1.3.2, Number 6:

Provide an assessment of the effects of gradually accumulating rubble on the drip shield response.

Basis: The drip shield is a free-standing structure that may be subjected to higher lateral-to-vertical load ratios during the early loading stages, leading to inward deformation of the legs that is not accounted in the current analyses.

1. RESPONSE

1.1 INTRODUCTION

Gradually accumulating rubble does not adversely affect the drip shield performance. It is demonstrated in this response that, although the drip shield legs can potentially slide on the invert more as a result of gradual rubble accumulation, the leg inclination, which is the important factor affecting load bearing capacity of the legs, is not underestimated in the detailed model in which the rubble pressure was applied instantaneously. The results of a simple two-dimensional model, in which gradual accumulation of rubble is simulated, are compared with detailed three-dimensional models used for analysis of drip shield stability and fragility.

The stability and structural integrity of the drip shield loaded by rubble in the collapsed emplacement drift in the lithophysal rock mass is analyzed for the six load realizations (e.g., BSC 2005, Table 5.2-2). Accumulation of relatively small blocks and static rubble load will be the dominant loading mechanism in the lithophysal units; dynamic impact of relatively large loose blocks will be dominant in the nonlithophysal rock mass, which is a stronger unit (BSC 2004, Section 6.4.2.5.1). The load realizations are specified as load distributions for 30 segments along the drip shield outline, in the counterclockwise direction starting with a segment at the bottom of the right leg and ending with the segment at the bottom of the left leg. There are ten segments along each leg and ten segments along the crown. The loads are obtained from the six simulations of drift collapse under quasi-static conditions (BSC 2004a, Section 6.4.2.5.3). The analysis used the numerical code UDEC. The lithophysal rock mass was represented as an assembly of polygonal (Voronoi) blocks. Because the objective of the calculations was an estimate of the rubble loads on the drip shield in the case of complete drift collapse, the collapse is induced, reducing the cohesive strength of rock mass to zero. The reduction was done gradually, in five equal increments. In the fifth increment, the cohesive strength of the rock mass was reduced to zero, and the drift completely collapsed. The objective of the UDEC simulations was to calculate rubble loads on the drip shield while drip shield deformation and stability under static conditions were analyzed in more detailed, three-dimensional models using the LS-DYNA and FLAC3D codes (e.g., BSC 2004b and BSC 2005). (LS-DYNA and FLAC3D, as documented in SNL 2007, Section 7.3.3.1, yield practically identical results for the drip shield statically loaded by rubble.) However, because of the effect of drip shield deformation on the interaction between the rubble and the drip shield, and on rubble loads, the stiffness of the drip shield representation in the UDEC model was calculated to properly represent deformability of the drip shield (BSC 2004a, Appendix Y). UDEC approximation overestimates stiffness of the lower portion of the drip shield leg, because it assumes constant leg thickness over the entire height.

This approximation should not have significant effect on the conclusions of this response. (The bending of the lower portion of the drip shield legs is underestimated, but the general mode of deformation and inclination of the legs are adequately represented. The approximation is taken into account in interpretation of the results.) The same friction coefficient between the drip shield leg and the invert of 0.4 was used in both the UDEC and FLAC3D calculations. The friction coefficient has the important effect on deformation of the drip shield legs during gradual accumulation of the rubble, because it will affect sliding of the leg base on the invert tuff.

Only the loads at the end of the UDEC simulations for a completely collapsed drift were used in the detailed analysis of drip shield stability. Those loads were applied instantaneously on the three-dimensional model of the drip shield. Gradual accumulation of rubble can cause more deformation of the drip shield legs as a result of sliding of the leg base on the crushed tuff, which is less likely to occur in the case of a completely collapsed drift and greater normal stress on the leg base because of greater load on the drip shield crown. The adverse effect of potential leg deformation on the drip shield load bearing capacity is initial inclination of the leg and increase in eccentricity of the vertical load that could reduce the leg buckling load.

The comparison of two models is conducted for material properties at 150°C and a drip shield configuration with 2-mm thinned plates, representative for first 10,000 years (BSC 2004b, Assumptions 3.7 and 3.8). The conclusions of this discussion should be valid for a range of similar conditions—i.e., until uniform corrosion causes sufficient thinning of the drip shield components that the rubble pressure due to partial drift collapse results in yielding of the drip shield legs.

1.2 DISCUSSION

Simulation of gradually decreasing strength (i.e., five increments of 20%) of the lithophysal rock mass also results in gradual accumulation of the rubble around the drip shield. *Drift Degradation Analysis* (BSC 2004a, Figure 6-171) illustrates the drift configuration and rubble accumulation as functions of percentage of the initial cohesive strength. In the UDEC calculations illustrated in *Drift Degradation Analysis* (BSC 2004a, Figure 6-171), the drip shield is assumed to be rigid with a rectangular outline. In the calculations from which the six load realizations were obtained (e.g., BSC 2004a, Figure 6-172), the drip shield is represented as deformable, with a more accurate representation of the geometry. Thus, although the objective of the UDEC simulations was not to analyze deformation of the drip shield, the simulations also represent the interaction between the drip shield and gradually accumulating rubble. The results of the UDEC simulations, which accounted for gradual accumulation of rubble, are used to assess the effect of gradually accumulating rubble on the drip shield response.

Figures 1 through 24, from simulations used to obtain the six rubble load realizations and to investigate drip shield deformation and stability, show the following information: (a) configuration of the drip shield and partially collapsed drift (a stage during simulation of drift collapse, typically 40 or 60% of the initial cohesive strength); (b) contours[1] of horizontal displacements for the stage of partially collapsed drift obtained from the UDEC model; (c) contours of horizontal displacement for completely collapsed drifts obtained from the UDEC model; and (d) contours of horizontal displacement for completely collapsed drifts obtained from the FLAC3D (i.e., detailed, three-dimensional) model in which the final rubble loads obtained from the UDEC model were applied instantaneously on the FLAC3D model. The FLAC3D results show the drip shield configurations and deformation states for the six rubble load realizations (same as those calculated in *Structural Stability of a Drip Shield Under Quasi-Static Pressure* (BSC 2004b) used as the initial states for analysis of drip shield creep deformation (BSC 2005)). Of particular interest, from the perspective of assessing the effect of gradual rubble accumulation, is the comparison of drip shield configurations and contours of horizontal displacement for a completely collapsed drift, obtained from UDEC (gradual rubble accumulation) and FLAC3D (instantaneous application of the final rubble loads) simulations.

The comparison indicates that FLAC3D models in which the rubble load is applied instantaneously, with fully developed vertical load on the drip shield crown, underestimate the potential for lateral sliding of the drip shield as a rigid body relative to the UDEC results in two analyzed cases. In load realizations 1 and 3, the rubble initially accumulates on one side of the drip shield, resulting in pushing of the drip shield laterally until it touches the pallet in the final configuration, when the drift completely collapses (e.g., Figures 3 and 11). However, this lateral sliding and rigid body movement is not associated with any deformation, and the drip shield practically maintains its original undeformed shape. A large unbalance of lateral load (load realizations 1 and 3) does not result in significant sliding of the drip shield in the FLAC3D model. Instead, the drip shield leans laterally (Figures 4 and 12). In the cases of load realizations 1 and 3 (compare Figures 3 and 4 for load realization 1, and Figures 11 and 12 for load realization 3), inclination of the drip shield legs, and eccentricity of the vertical load in the legs, predicted from the FLAC3D models is much greater than those predicted from the UDEC models, which accounted for gradual rubble accumulation. For load realization 3, the left leg in the FLAC3D model bends approximately 16 cm to the inside, relative to the drip shield shoulder. Thus, in the cases in which the UDEC model predicts lateral rigid body translation of the drip shield, the FLAC3D model results in more unfavorable configuration of the drip shield with respect to its load bearing capacity.

For load realizations 2 and 4, the UDEC and FLAC3D models show, qualitatively, the same mode of deformation (Figures 7 and 8 for load realization 2 and Figures 15 and 16 for load realization 4). Both cases indicate bending of the right drip shield leg inward. In load realization 2, as predicted from the FLAC3D model, the right leg bends inside approximately 20 cm relative to the drip shield shoulder, compared to 12 cm observed from the results of the

[1] The contours in the figures represent the horizontal displacement field. The displacements are provided in meters. Each figure includes a scale which covers the range of displacements between the minimum and the maximum for the particular model. The range is divided in a number of intervals, which are assigned different colors. The colors help visually determine displacements of different points of the model.

UDEC model, which underestimates displacements because of approximation of the stiffness of the lower portion of the drip shield leg. Instantaneous application of the rubble load for collapsed drift does not affect drip shield load bearing capacity for load realizations 2 and 4.

For load realizations 5 and 6, the mode of drip shield deformation is affected by the loading sequence. The rubble accumulates relatively symmetrically (Figures 17 and 21) and, as a result, the UDEC model predicts that both legs move inward (Figures 19 and 23). Because of the loading sequence and frictional resistance at the leg base, the FLAC3D model (Figures 20 and 24) predicts less lateral movement of the right leg, which, for load realization 5 (Figure 19), is calculated in the UDEC model to be approximately 15 cm. However, for load realization 5, the FLAC3D model predicts outward bending of the right leg of 9 cm and inward bending of the left leg of approximately 5 cm. In load realization 6, inward deformation of the left leg in the FLAC3D model is approximately 8 cm (Figure 24), compared to 8 cm of inward deformation of the right leg predicted from the UDEC model (Figure 23).

All of the calculations were carried out for a friction coefficient between the invert and the drip shield legs of 0.4 (e.g., BSC 2005, Section 3.2.2). Although the metal-to-stone friction coefficient is typically between 0.3 and 0.7, it is expected that in the case of crushed tuff and uneven settlement of the invert (which will occur with time), the effective friction angle will be close to 0.7 or greater. (When the steel substructure in the invert degrades as a result of corrosion, the drip shield legs can penetrate into the crushed tuff, which will increase resistance to lateral displacement of the legs; see the response to RAI 3.2.2.1.3.2-005.) Thus, the presented calculations overestimate the potential for sliding of the drip shield legs on the invert and their inward deformation. Increase in the friction coefficient will increase reaction force at the drip shield leg base (acting in opposite direction to the load on the leg) and, consequently, result in reduced leg deformation. Thus, although the mode of deformation is different, the leg eccentricity predicted from the two different models is similar. The gradual rubble accumulation does not have a significant effect on the drip shield load bearing capacity, even in rubble load realizations 5 and 6.

In the analysis of the drip shield framework fragility (SNL 2007, Section 6.4.3.2), the initial lateral displacements of the drip shield legs are less than those shown in Figures 4, 8, 12, 16, 20, and 24, because in this model the horizontal springs are used to represent reactive rubble pressure along the drip shield legs (besides the active loads applied on the drip shield legs). However, the purpose of the drip shield fragility analyses presented in *Mechanical Assessment of Degraded Waste Packages and Drip Shields Subject to Vibratory Ground Motion* (SNL 2007, Section 6.4.3.2) was to determine the vertical failure load to be correlated to vertical peak ground acceleration in order to determine the ground motion intensity at which the framework collapses. The objective was to provide bounding estimates using relatively simple quasi-static calculations, without analyzing complex process of dynamic rubble–structure interaction in three dimensions. Comparison with results of dynamic simulations (SNL 2007, Section 6.4.4) indicates that quasi-static fragility calculations are appropriate for bounding estimates because they lead to drip shield collapse at lesser loads than comparable dynamic simulations.

1.3 CONSISTENCY WITH RELATED FEPS

In the load bearing capacity analysis of the drip shield, the rubble load for completely collapsed drift is instantaneously applied on the drip shield. This is a physically reasonable approach for the drip shield capacity assessment. This approach is not relevant to the screening justifications for excluded FEPs 2.1.07.05.0B, Creep of Metallic Materials in the Drip Shield; 2.1.03.03.0B, Localized Corrosion of Drip Shields; 2.1.06.05.0B, Mechanical Degradation of Invert; and 2.1.07.06.0A, Floor Buckling.

1.4 SUMMARY

Although the loading sequence that would result from gradual rubble accumulation was not simulated explicitly in the LS-DYNA (BSC 2004b) and FLAC3D (BSC 2005) analyses of drip shield response, the effect of deformation of the drip shield legs on drip shield stability is properly accounted for. The FLAC3D model shows inward deformation of the drip shield legs (either due to their sliding or due to leaning of the entire drip shield), which is typically the same as or exceeds the deformation calculated from the UDEC model that accounts for the loading sequence as a result of gradual rubble accumulation. Gradual accumulation of the rubble will not adversely affect drip shield performance or its load bearing capacity. Because the statically loaded drip shield represents the initial state for analysis of the drip shield creep deformation, gradual accumulation of the rubble will not affect the conclusions of the creep simulations and exclusion of FEP 2.1.07.05.0B.

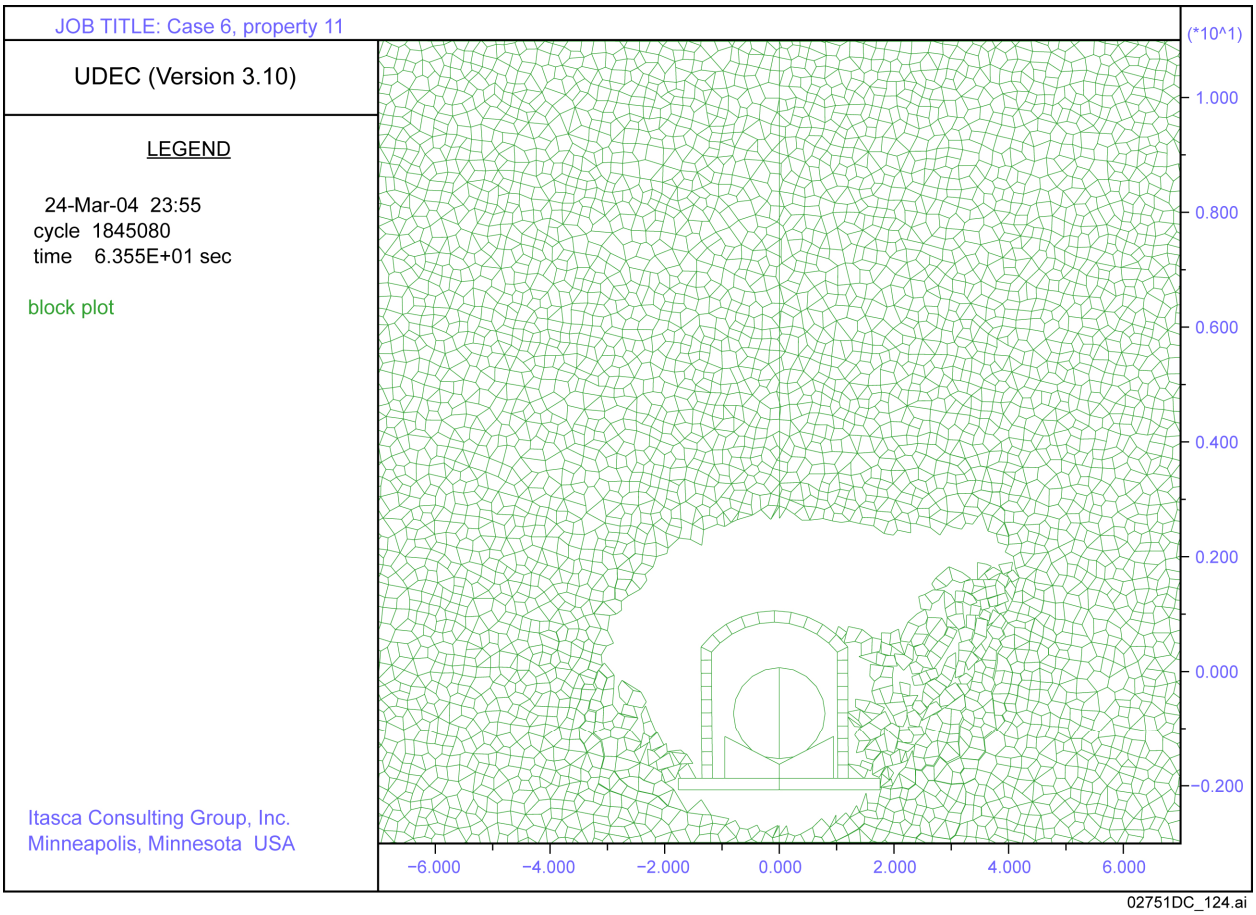

Figure 1. Realization 1: State of Partial Drift Collapse after 40% of Strength Reduction (units are meters)

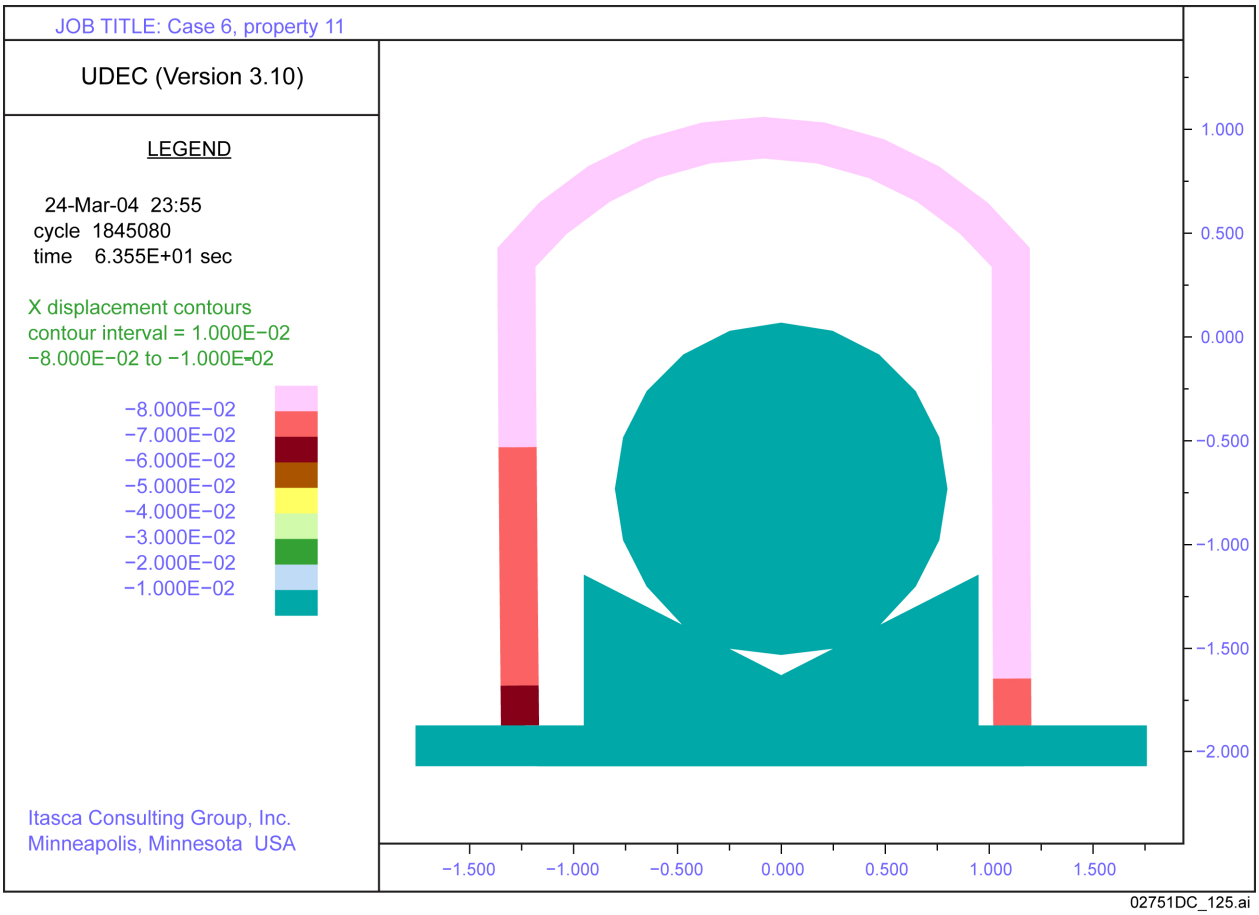

NOTE: Units are meters; positive displacements are to the right.

Figure 2. Realization 1: Drip Shield Configuration and Contours of Horizontal Displacements at State of Partial Drift Collapse Calculated in UDEC Model

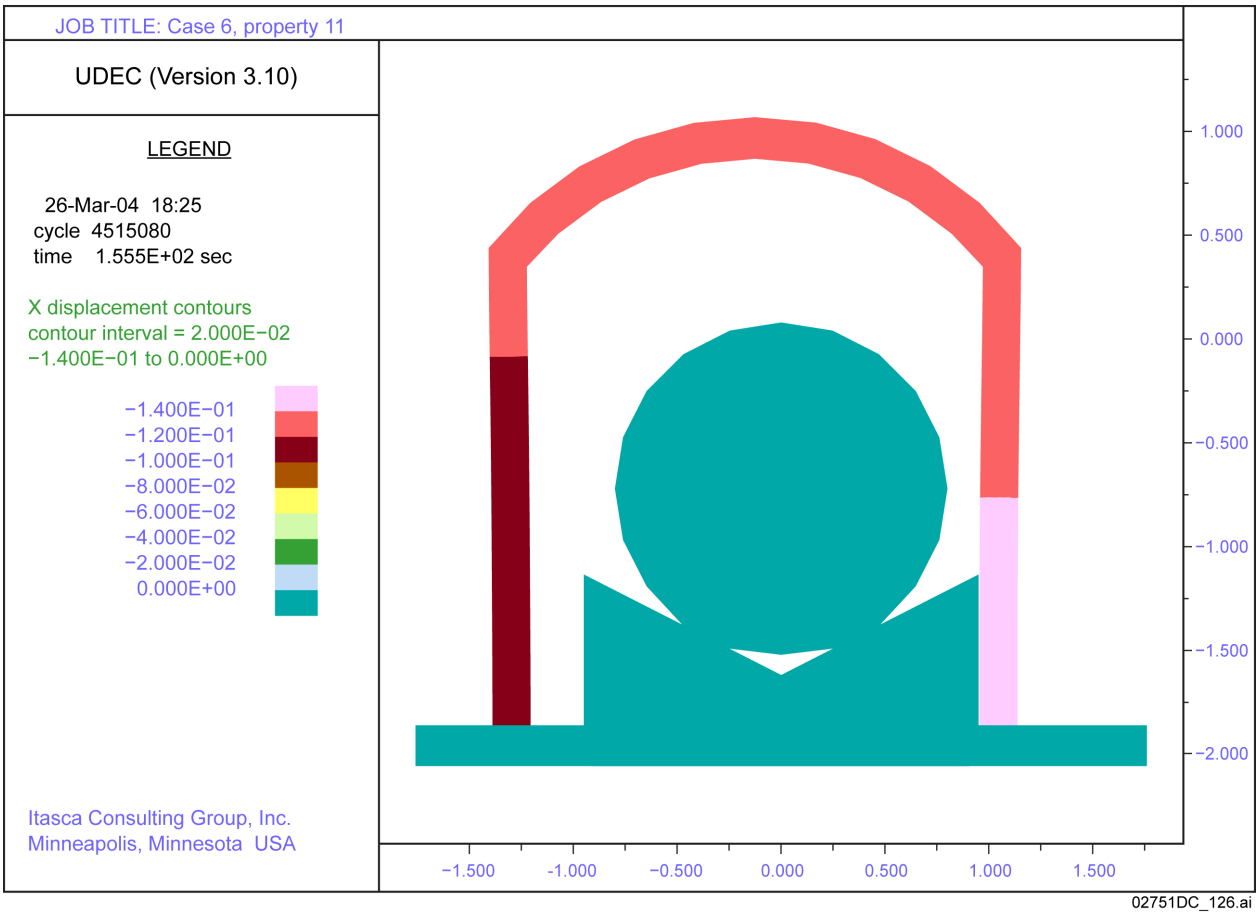

NOTE: Units are meters; positive displacements are to the right.

Figure 3. Realization 1: Drip Shield Configuration and Contours of Horizontal Displacements at State of Complete Drift Collapse Calculated in UDEC Model

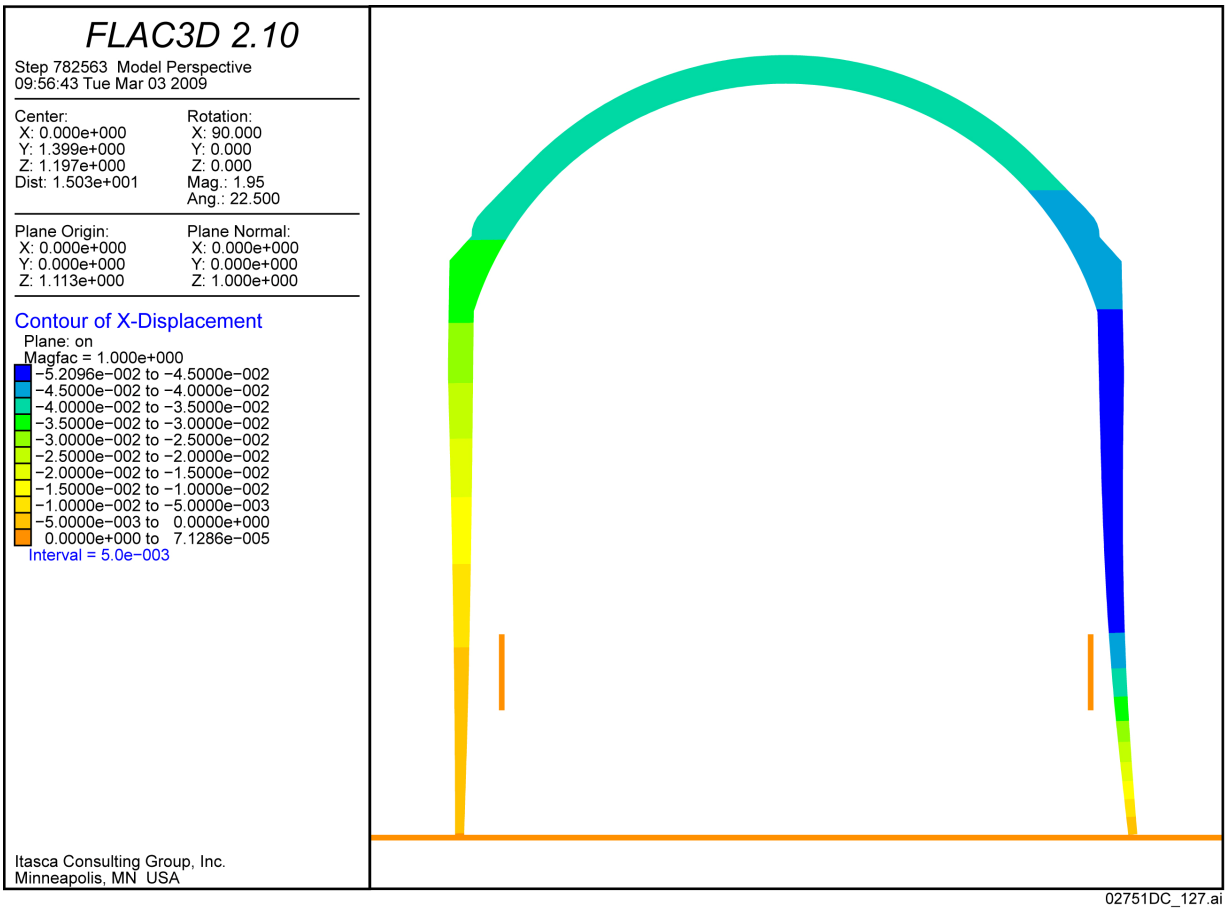

NOTE: Units are meters; positive displacements are to the right.

Figure 4. Realization 1: Drip Shield Configuration and Contours of Horizontal Displacements at State of Complete Drift Collapse Calculated in FLAC3D Model

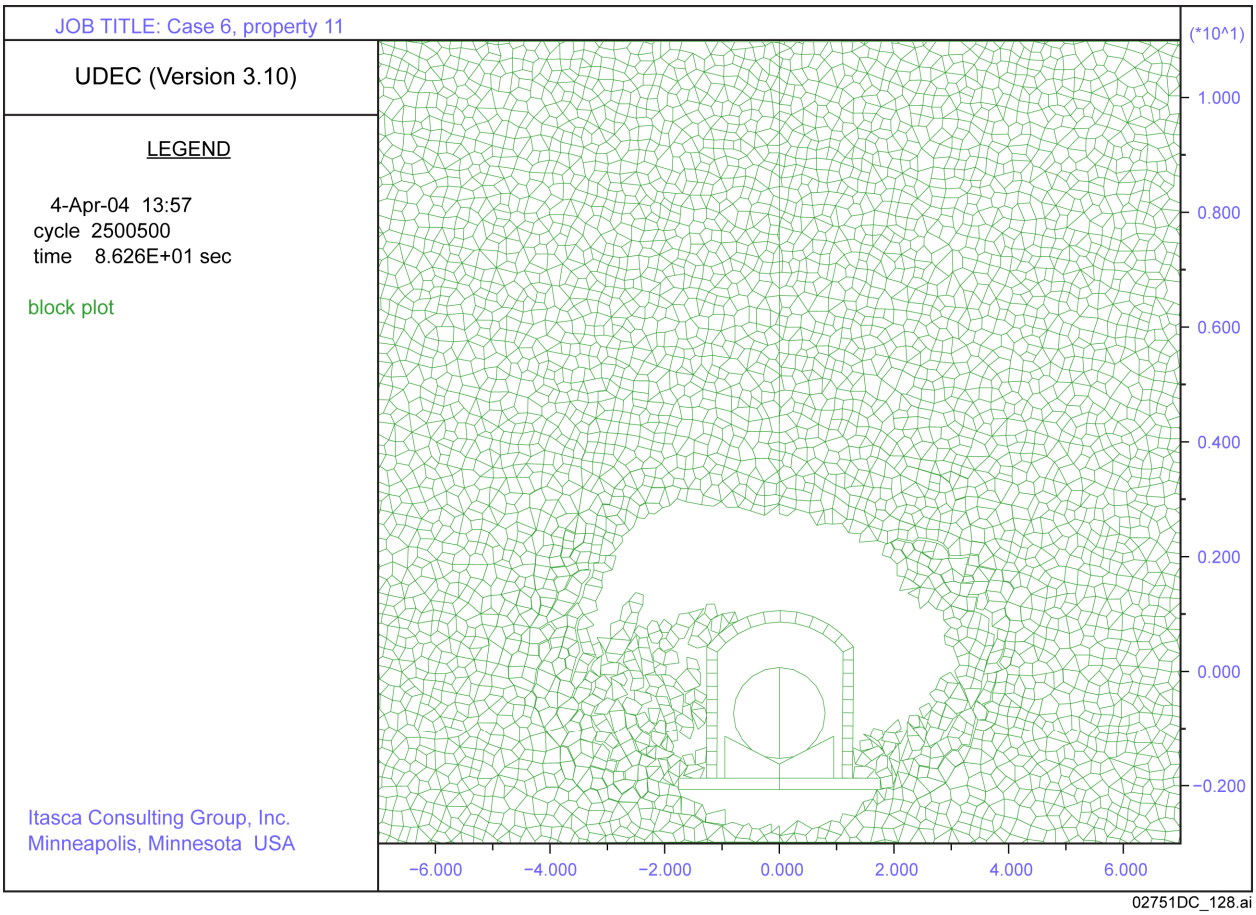

Figure 5. Realization 2: State of Partial Drift Collapse after 60% of Strength Reduction (units are meters)

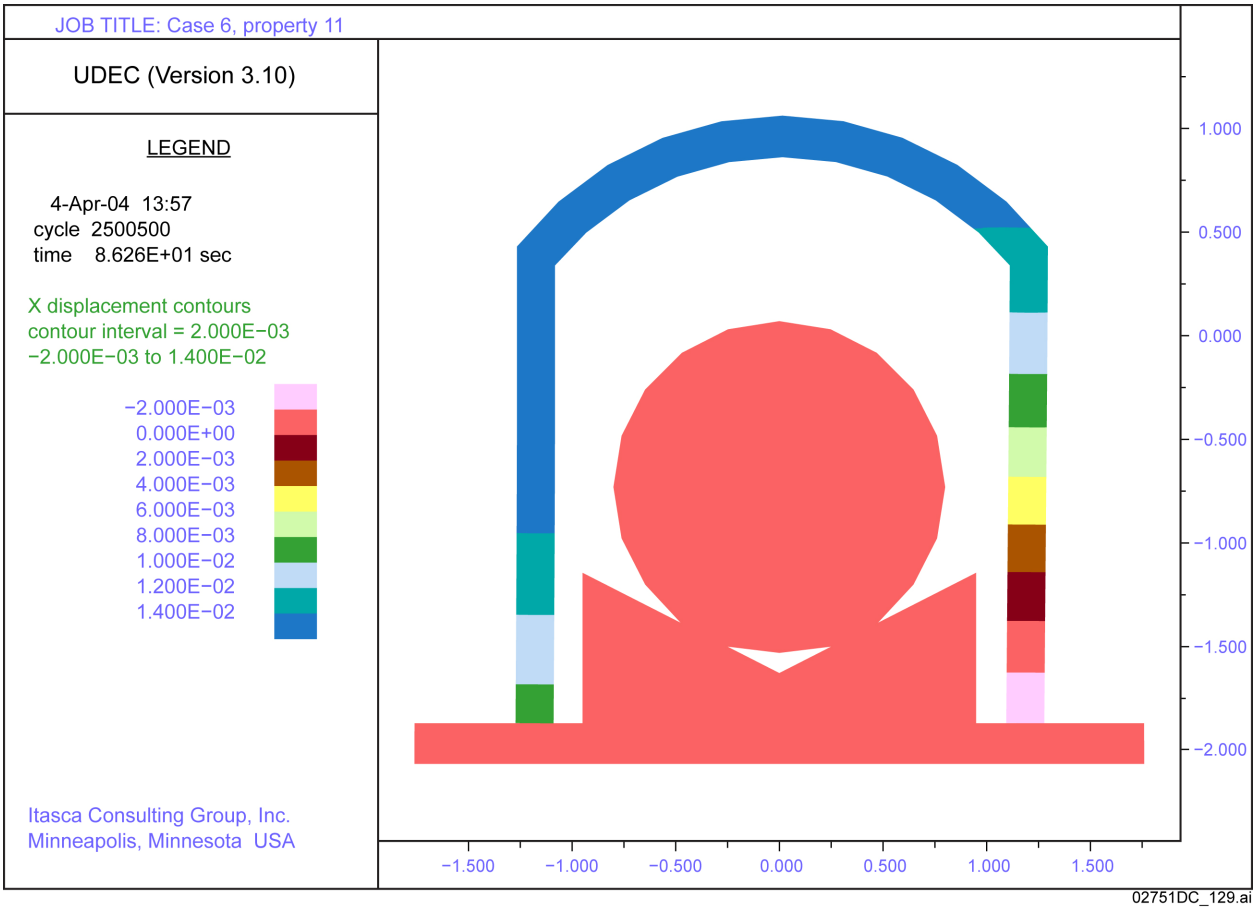

NOTE: Units are meters; positive displacements are to the right.

Figure 6. Realization 2: Drip Shield Configuration and Contours of Horizontal Displacements at State of Partial Drift Collapse Calculated in UDEC Model

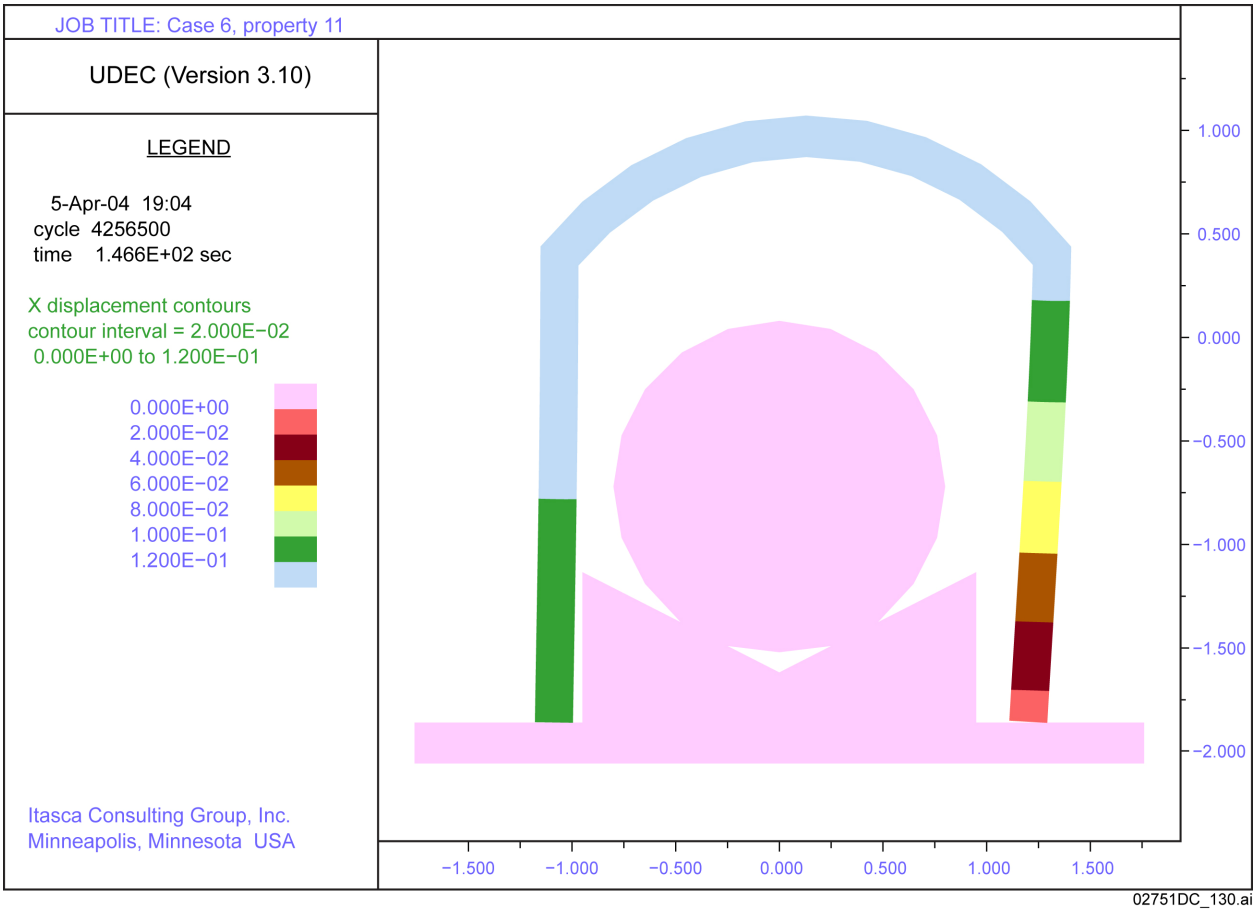

NOTE: Units are meters; positive displacements are to the right.

Figure 7. Realization 2: Drip Shield Configuration and Contours of Horizontal Displacements at State of Complete Drift Collapse Calculated in UDEC Model

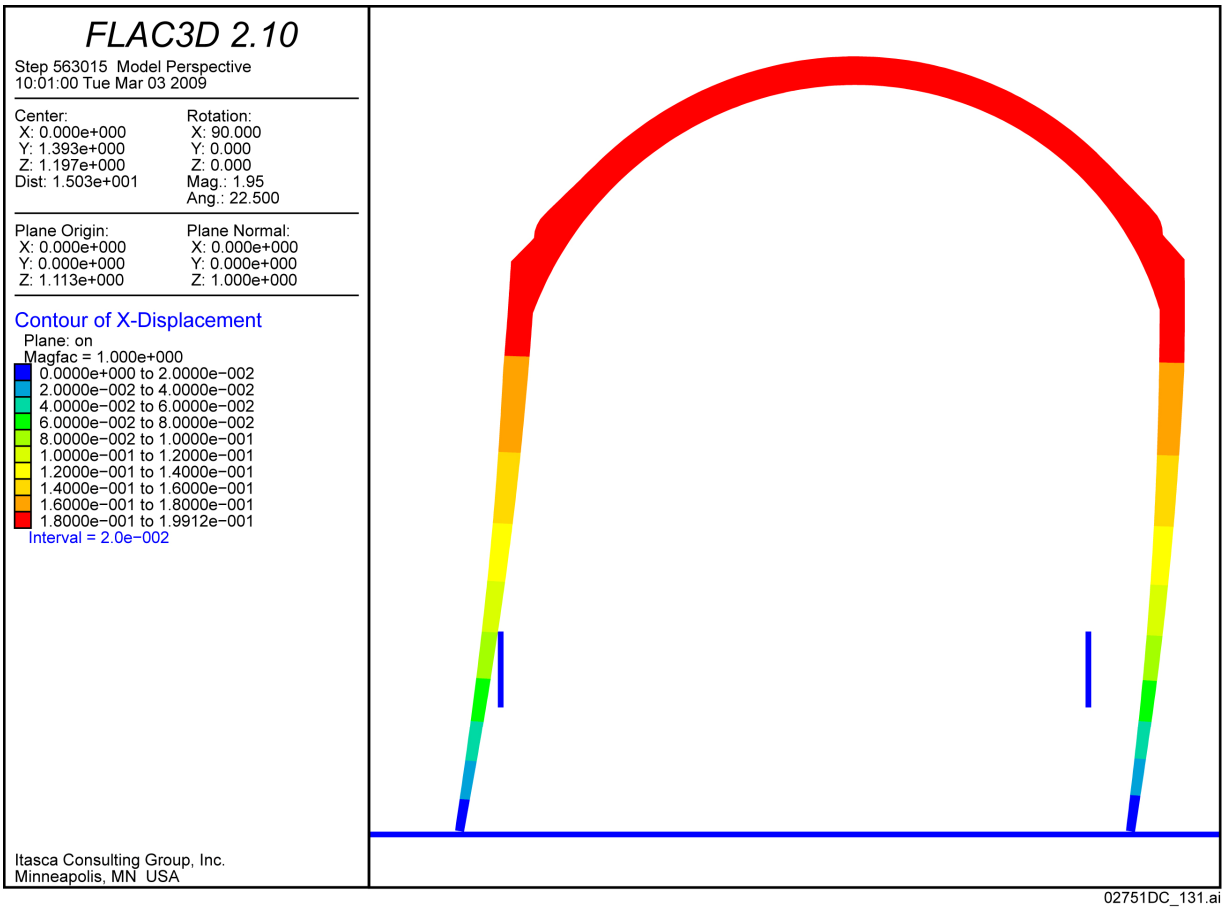

NOTE: Units are meters; positive displacements are to the right.

Figure 8. Realization 2: Drip Shield Configuration and Contours of Horizontal Displacements at State of Complete Drift Collapse Calculated in FLAC3D Model

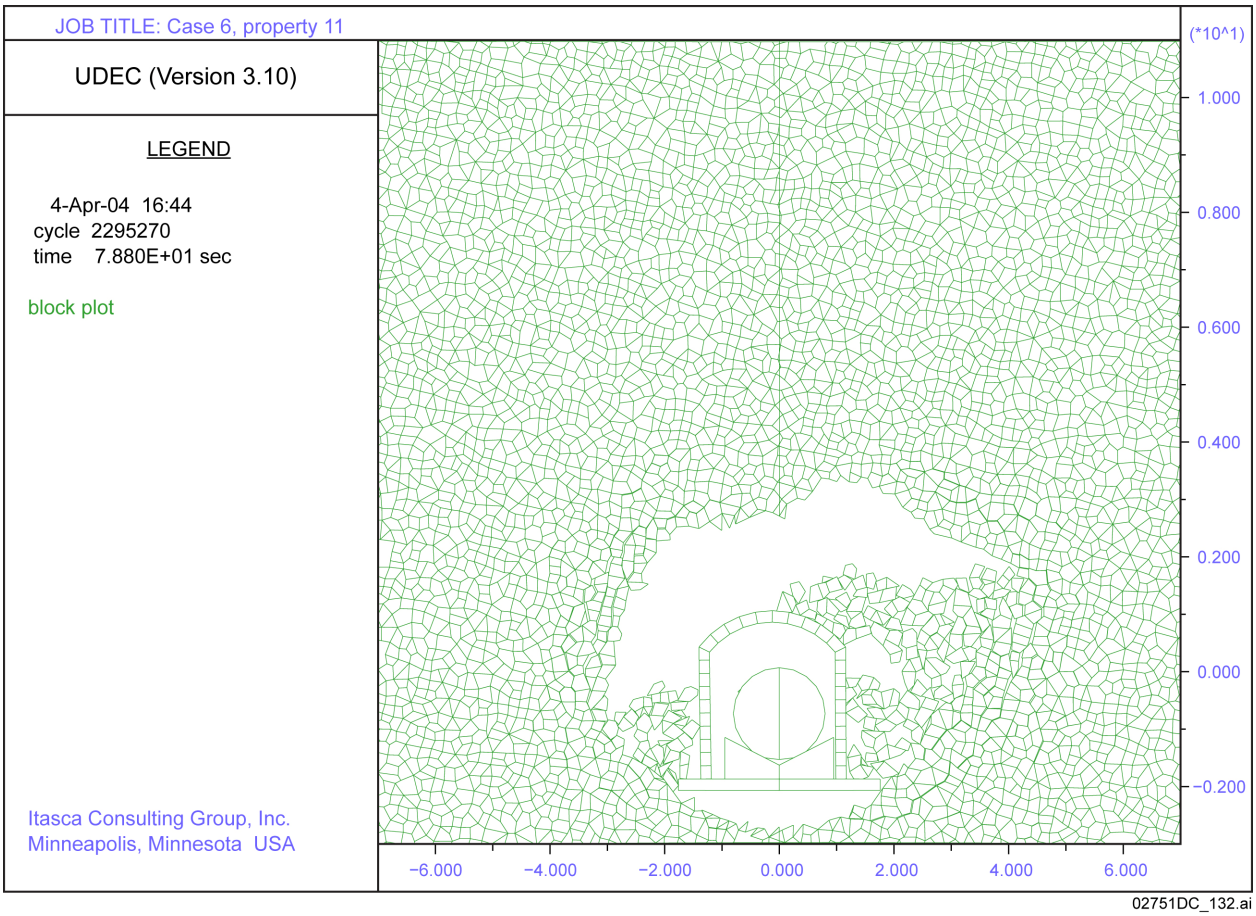

Figure 9. Realization 3: State of Partial Drift Collapse after 60% of Strength Reduction (units are meters)

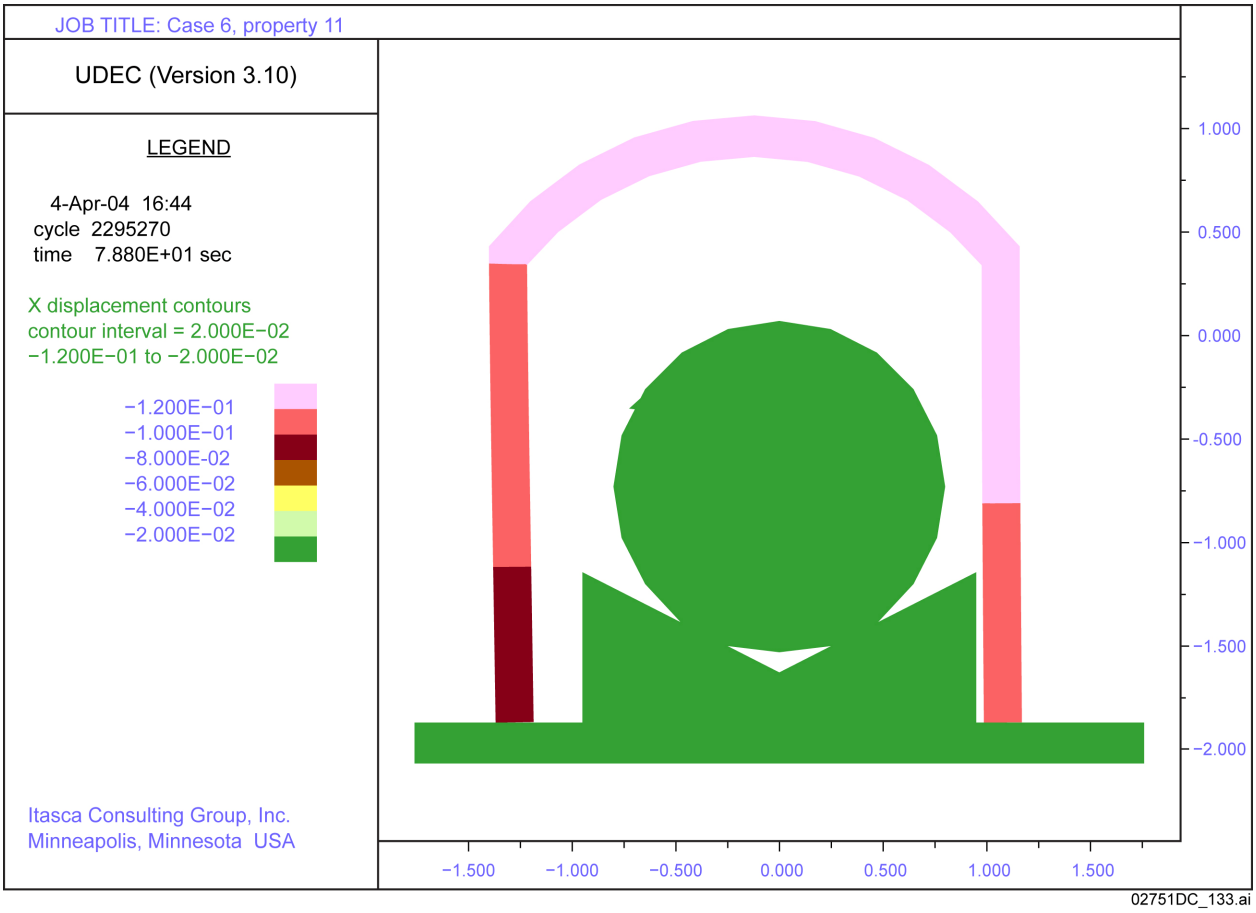

NOTE: Units are meters; positive displacements are to the right.

Figure 10. Realization 3: Drip Shield Configuration and Contours of Horizontal Displacements at State of Partial Drift Collapse Calculated in UDEC Model

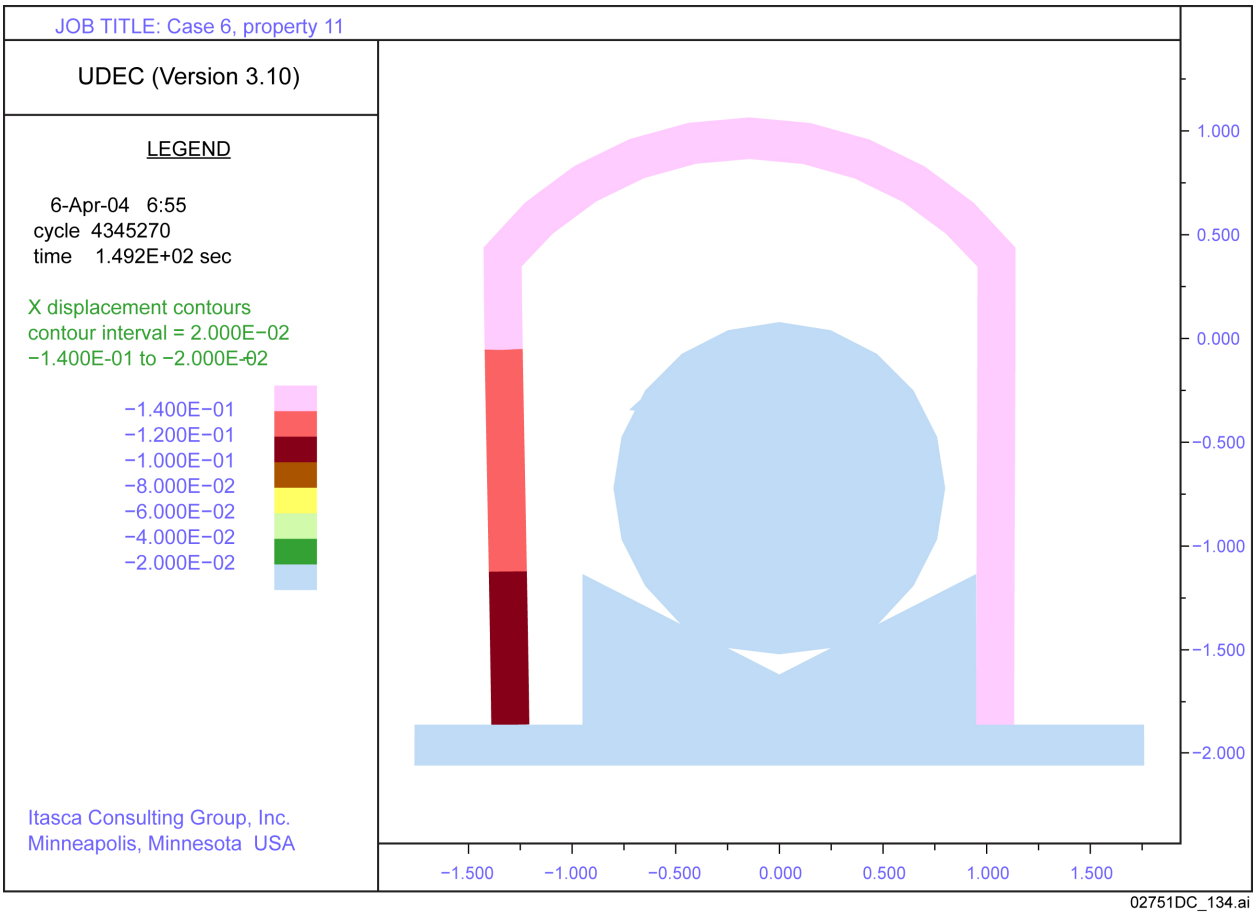

NOTE: Units are meters; positive displacements are to the right.

Figure 11. Realization 3: Drip Shield Configuration and Contours of Horizontal Displacements at State of Complete Drift Collapse Calculated in UDEC Model

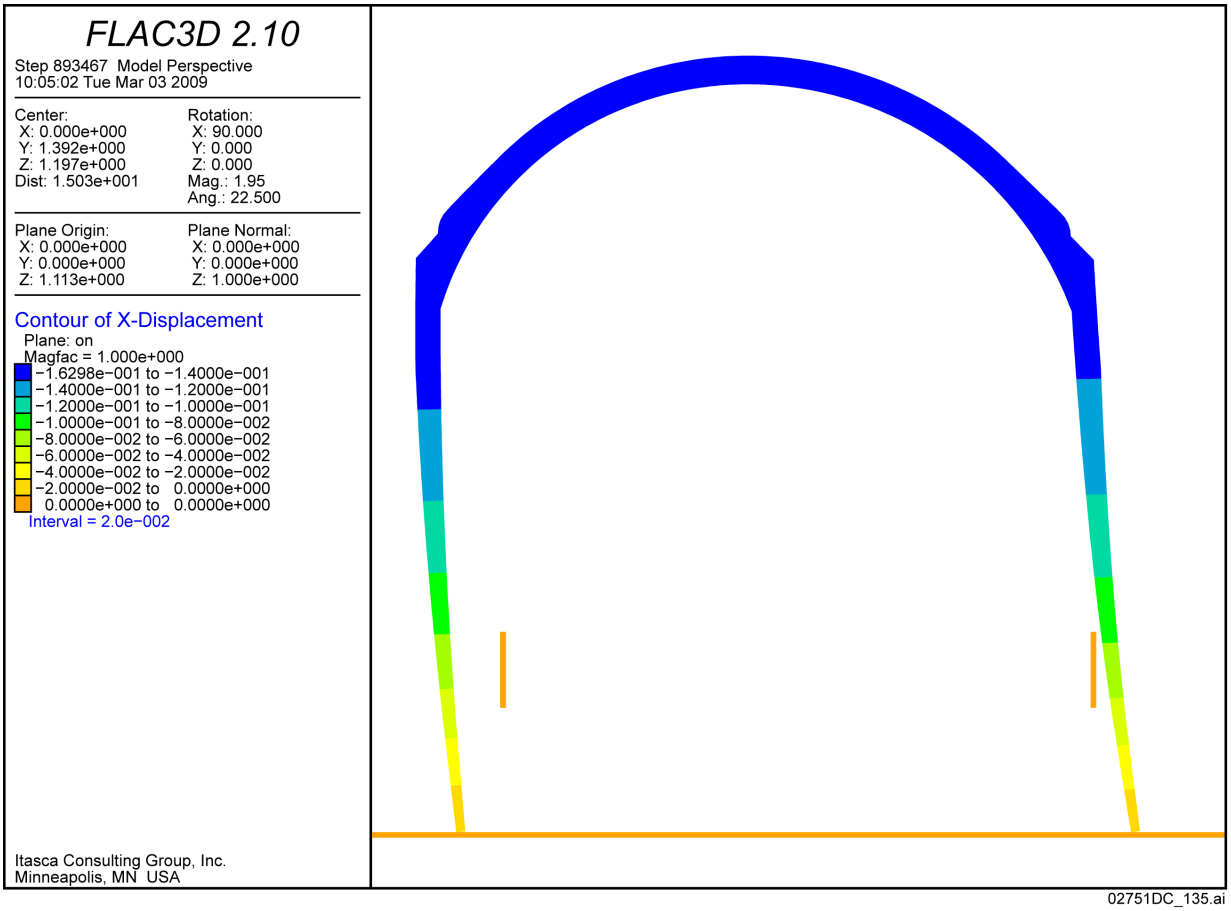

NOTE: Units are meters; positive displacements are to the right.

Figure 12. Realization 3: Drip Shield Configuration and Contours of Horizontal Displacements at State of Complete Drift Collapse Calculated in FLAC3D Model

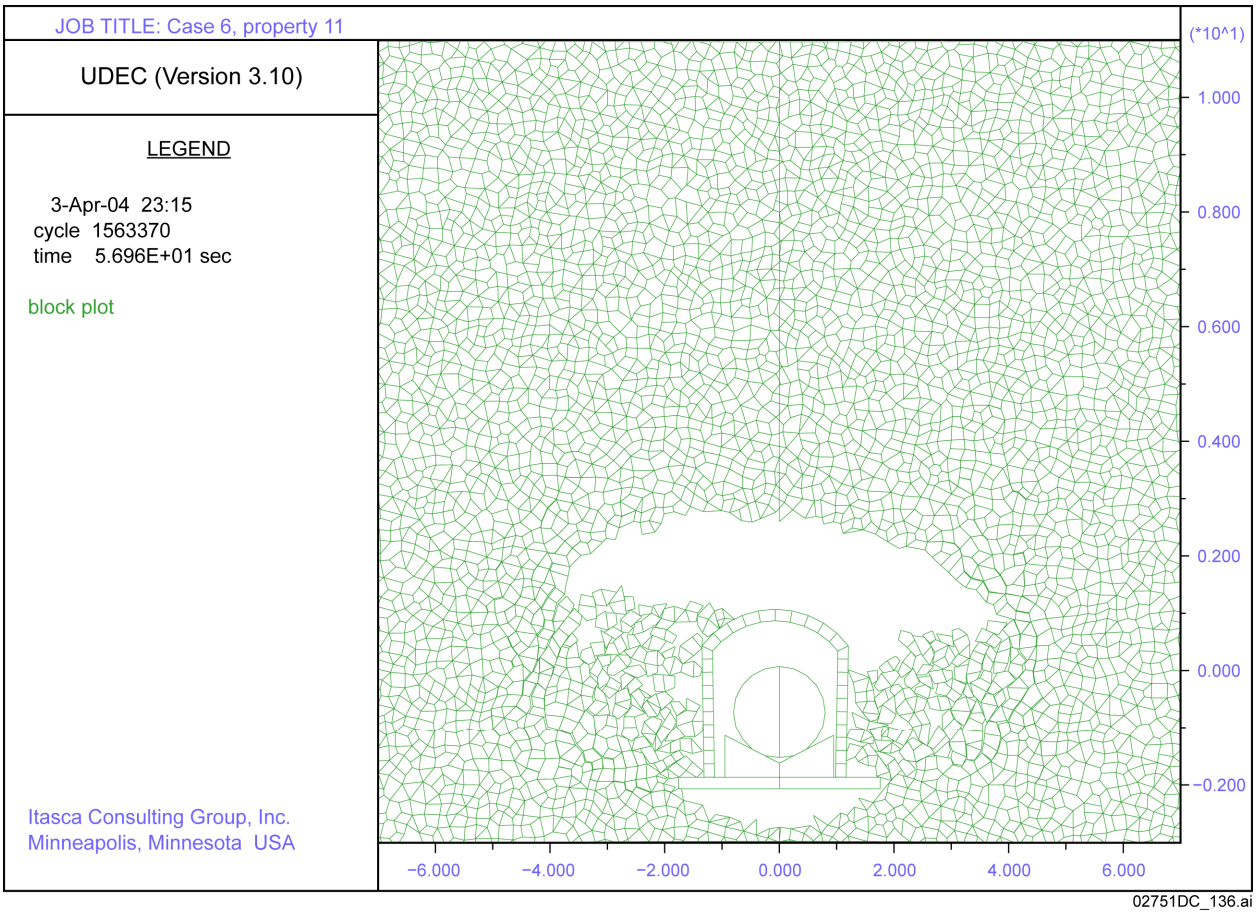

Figure 13. Realization 4: State of Partial Drift Collapse after 40% of Strength Reduction (units are meters)

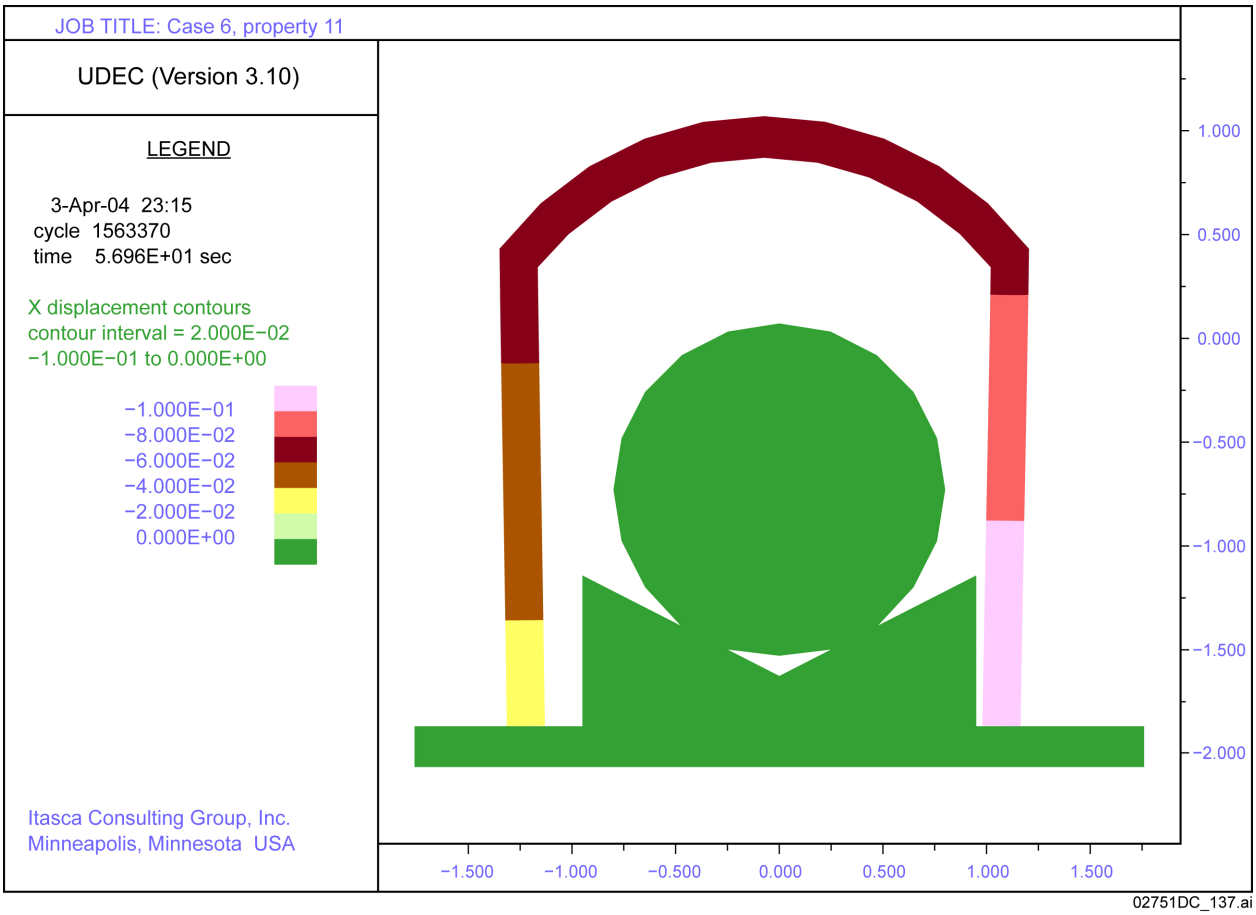

NOTE: Units are meters; positive displacements are to the right.

Figure 14. Realization 4: Drip Shield Configuration and Contours of Horizontal Displacements at State of Partial Drift Collapse Calculated in UDEC Model

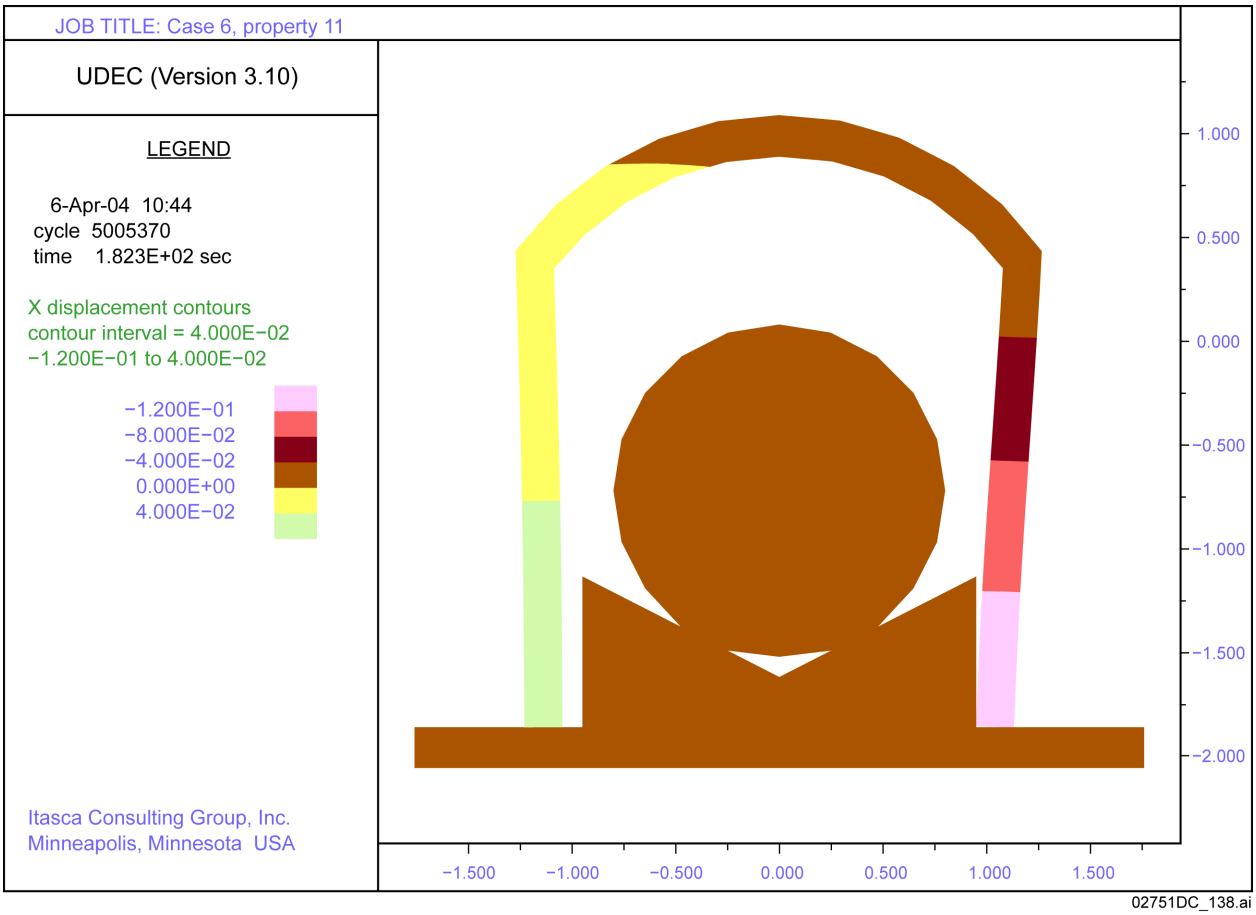

NOTE: Units are meters; positive displacements are to the right.

Figure 15. Realization 4: Drip Shield Configuration and Contours of Horizontal Displacements at State of Complete Drift Collapse Calculated in UDEC Model

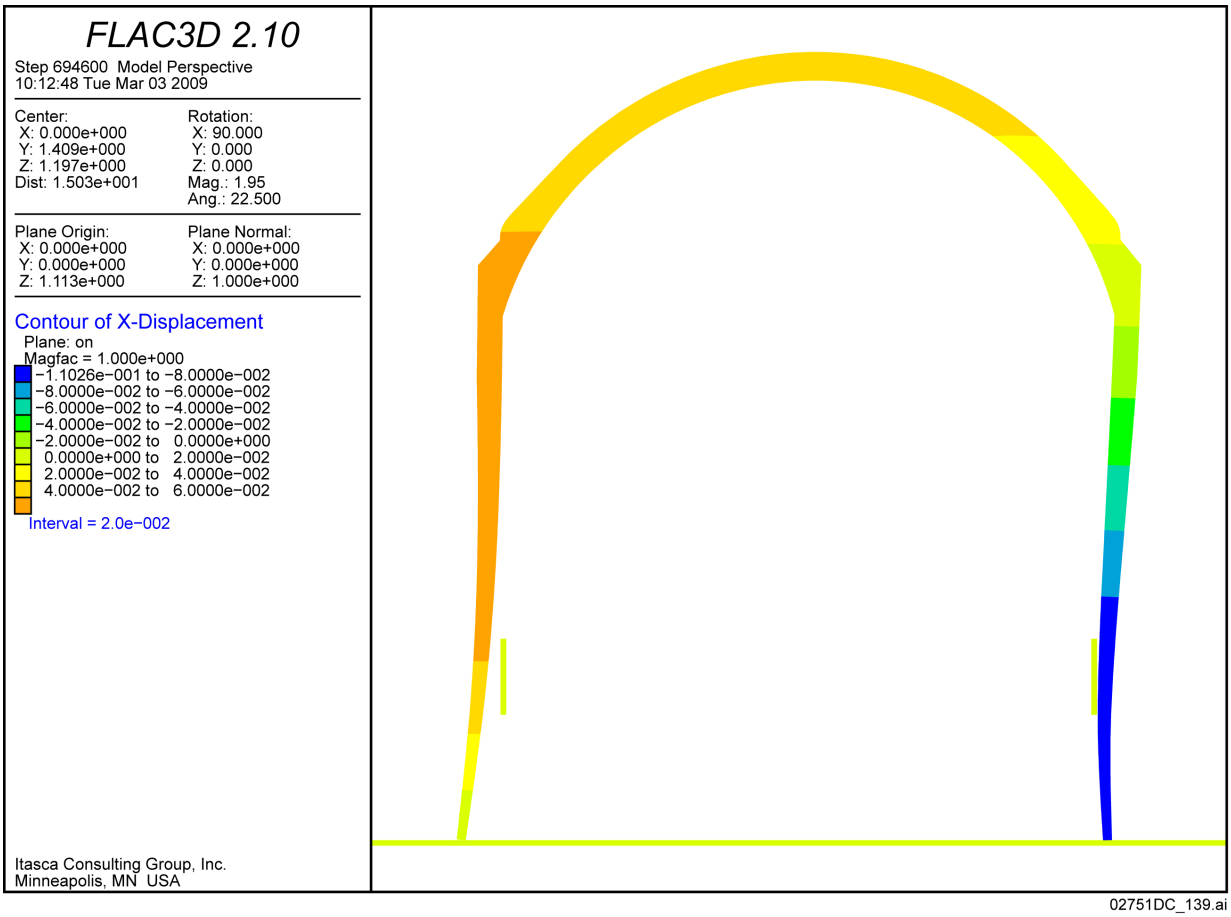

NOTE: Units are meters; positive displacements are to the right.

Figure 16. Realization 4: Drip Shield Configuration and Contours of Horizontal Displacements at State of Complete Drift Collapse Calculated in FLAC3D Model

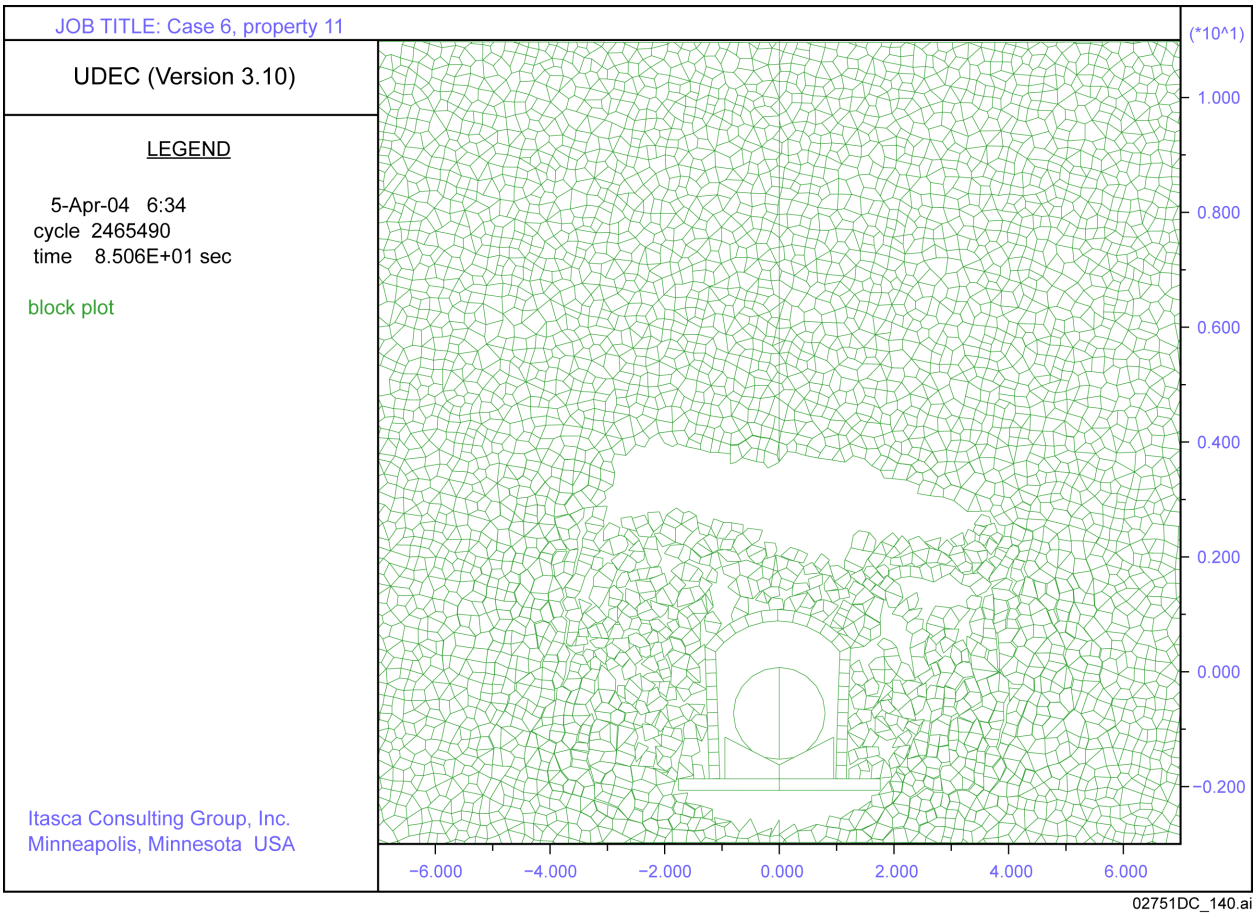

Figure 17. Realization 5: State of Partial Drift Collapse after 60% of Strength Reduction (units are meters)

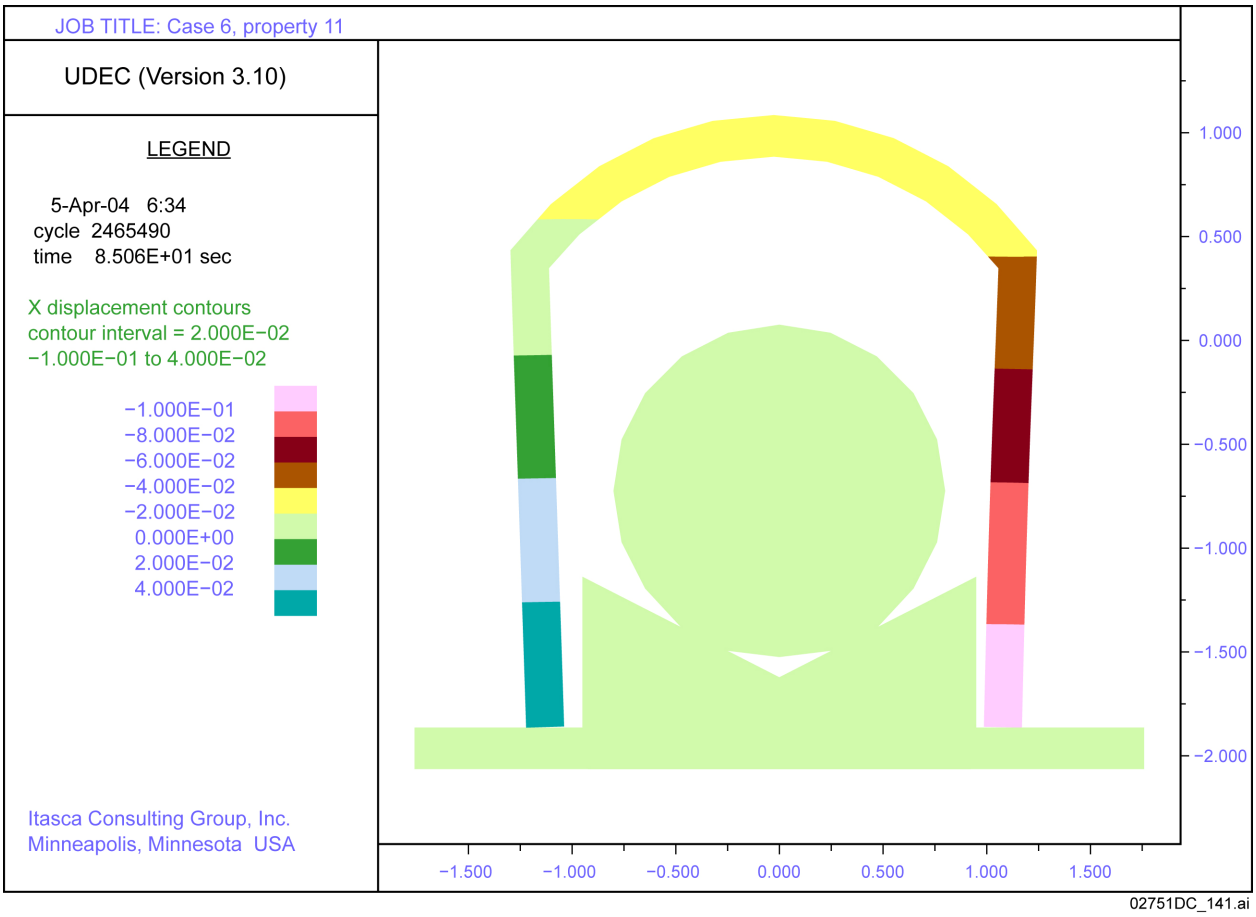

NOTE: Units are meters; positive displacements are to the right.

Figure 18. Realization 5: Drip Shield Configuration and Contours of Horizontal Displacements at State of Partial Drift Collapse Calculated in UDEC Model

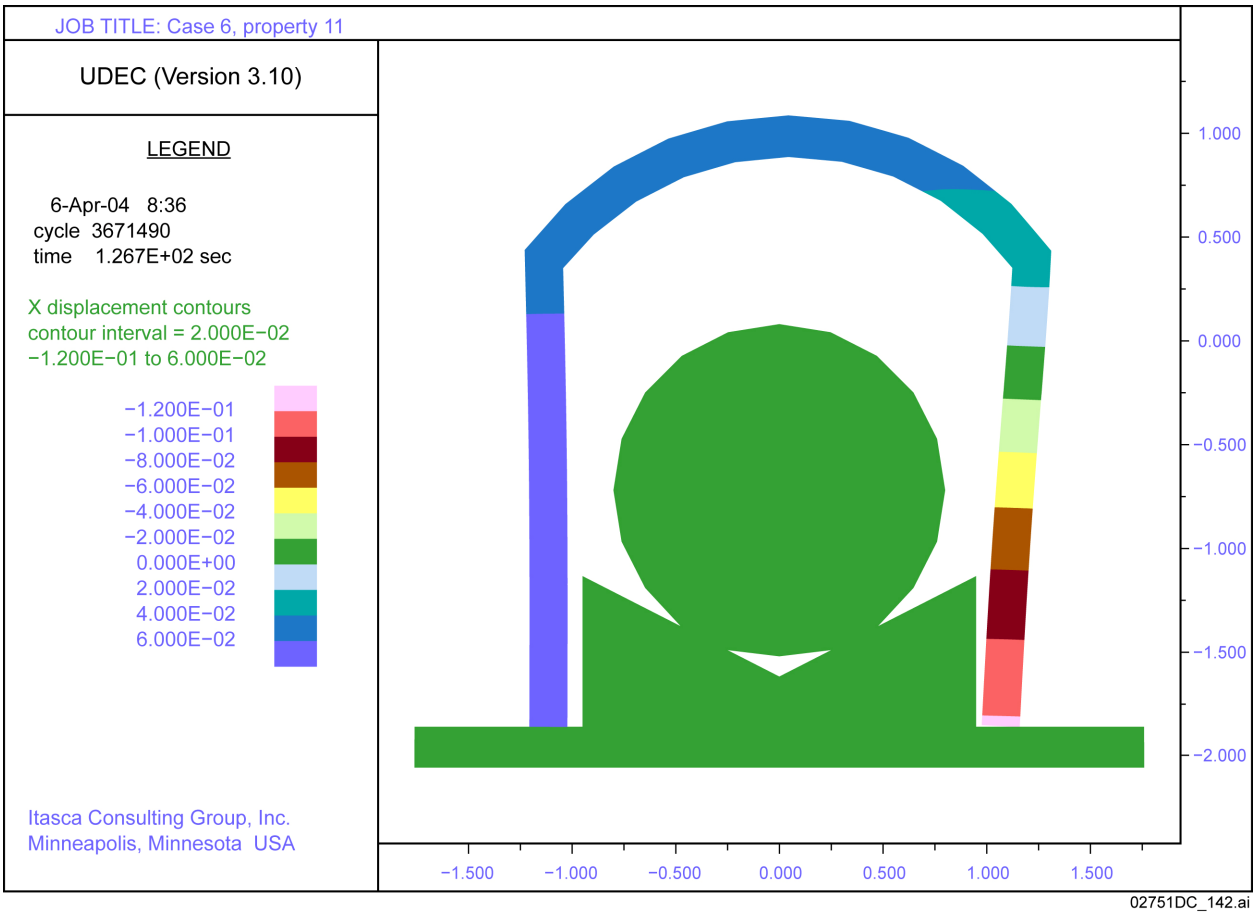

NOTE: Units are meters; positive displacements are to the right.

Figure 19. Realization 5: Drip Shield Configuration and Contours of Horizontal Displacements at State of Complete Drift Collapse Calculated in UDEC Model

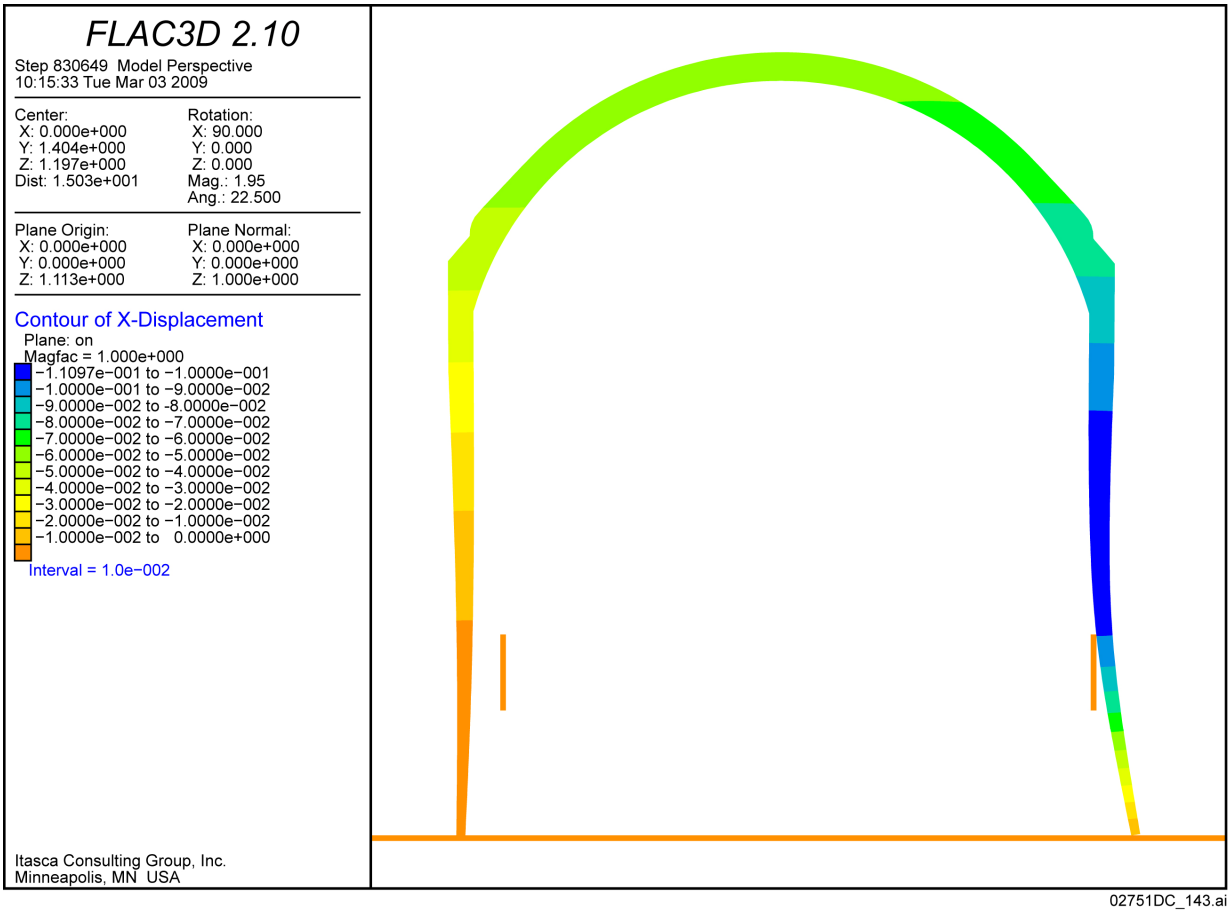

NOTE: Units are meters; positive displacements are to the right.

Figure 20. Realization 5: Drip Shield Configuration and Contours of Horizontal Displacements at State of Complete Drift Collapse Calculated in FLAC3D Model

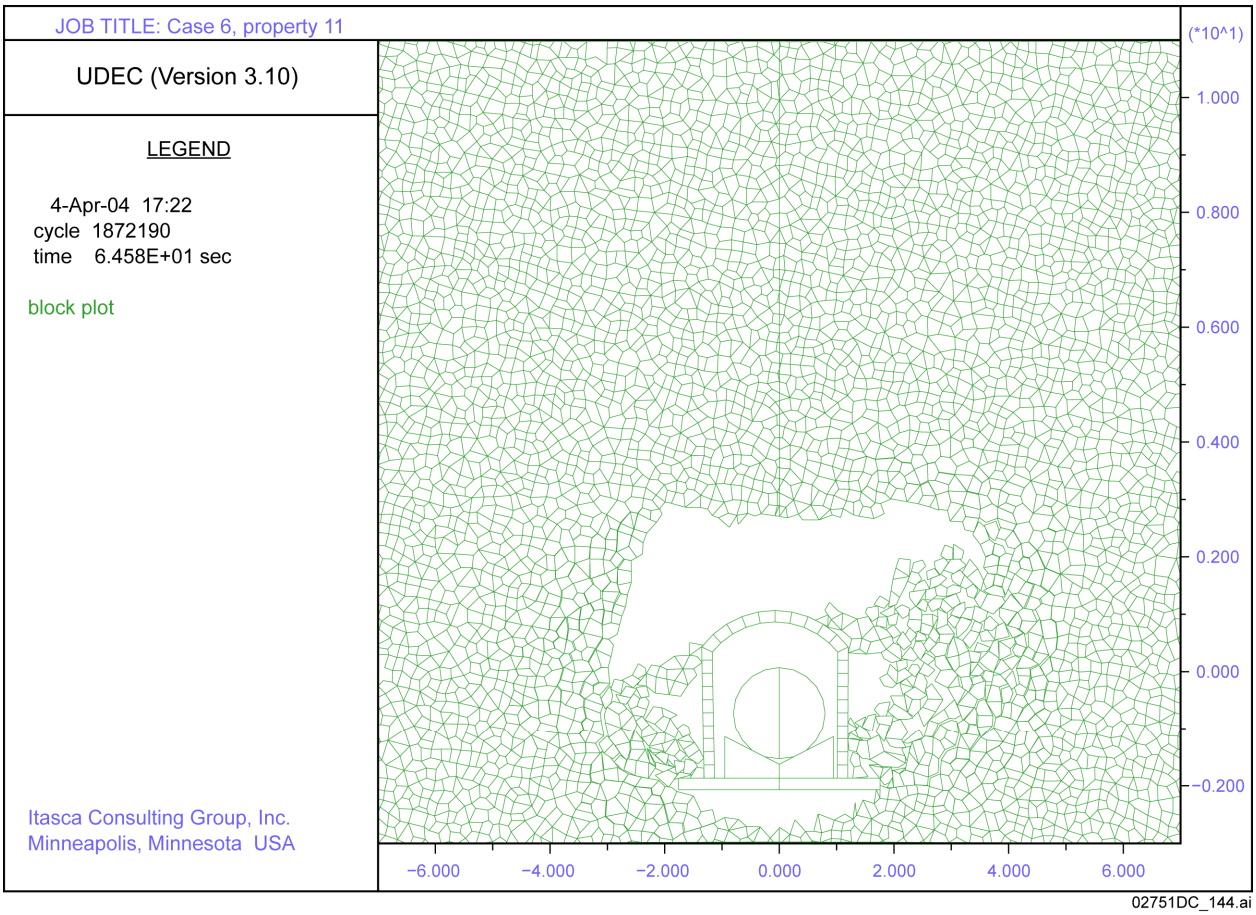

Figure 21. Realization 6: State of Partial Drift Collapse after 60% of Strength Reduction (units are meters)

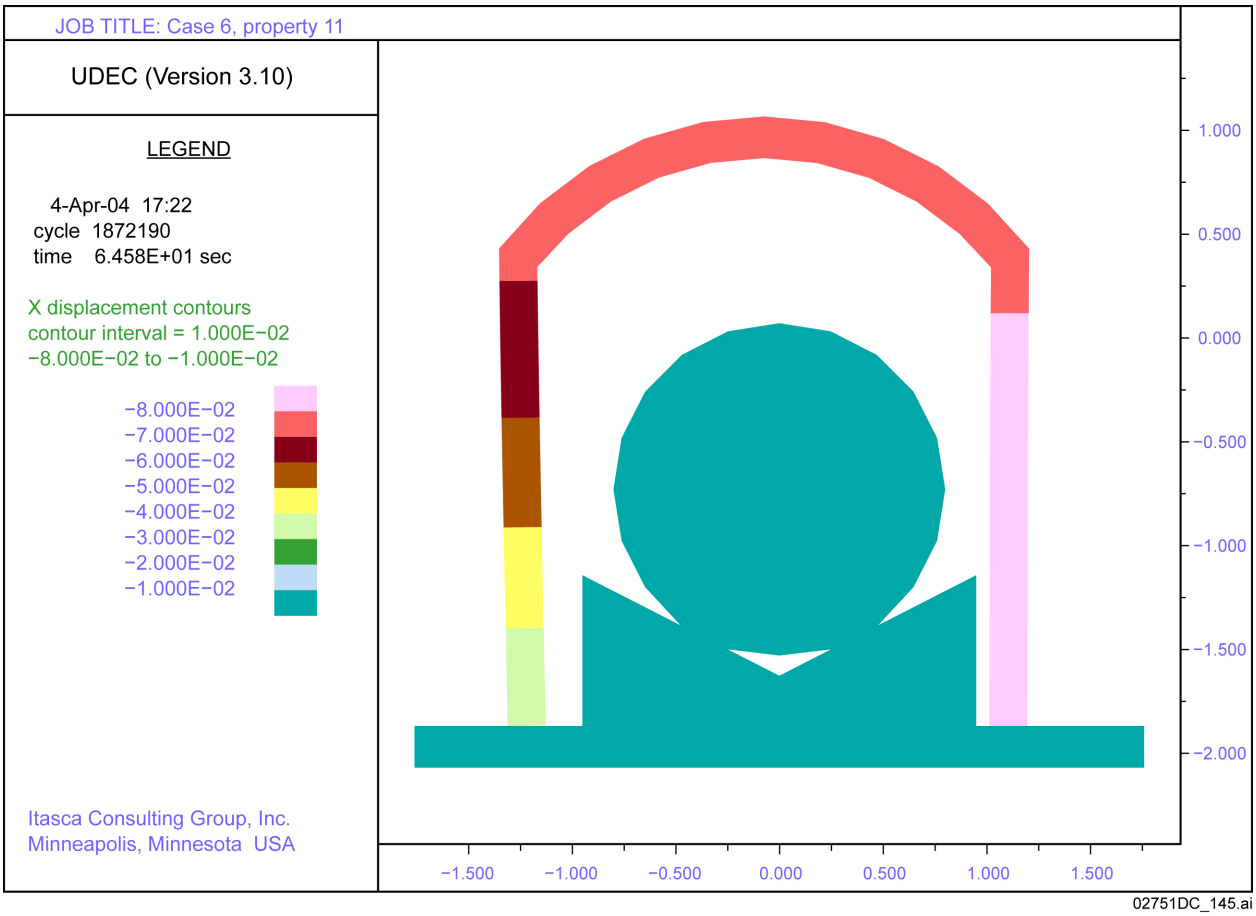

NOTE: Units are meters; positive displacements are to the right.

Figure 22. Realization 6: Drip Shield Configuration and Contours of Horizontal Displacements at State of Partial Drift Collapse Calculated in UDEC Model

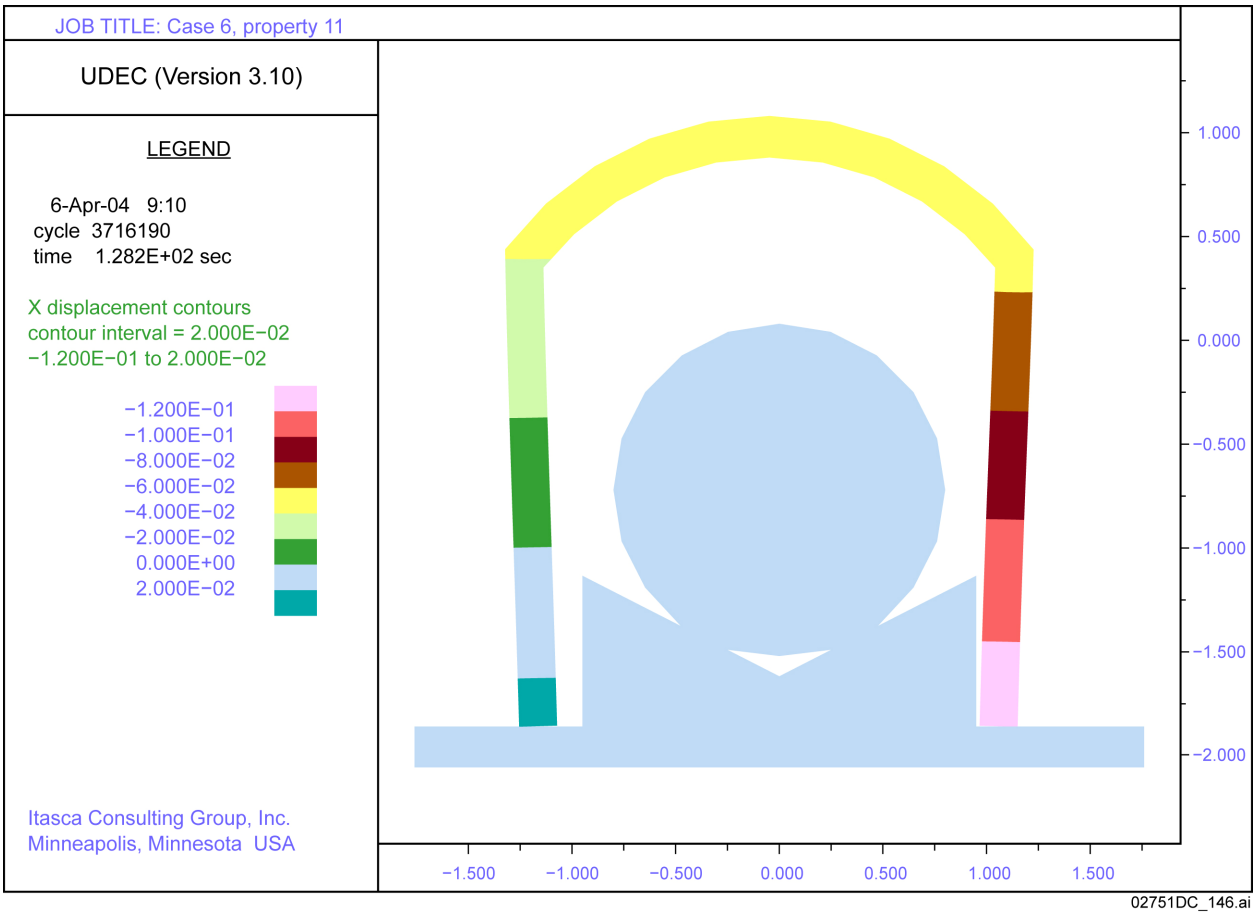

NOTE: Units are meters; positive displacements are to the right.

Figure 23. Realization 6: Drip Shield Configuration and Contours of Horizontal Displacements at State of Complete Drift Collapse Calculated in UDEC Model

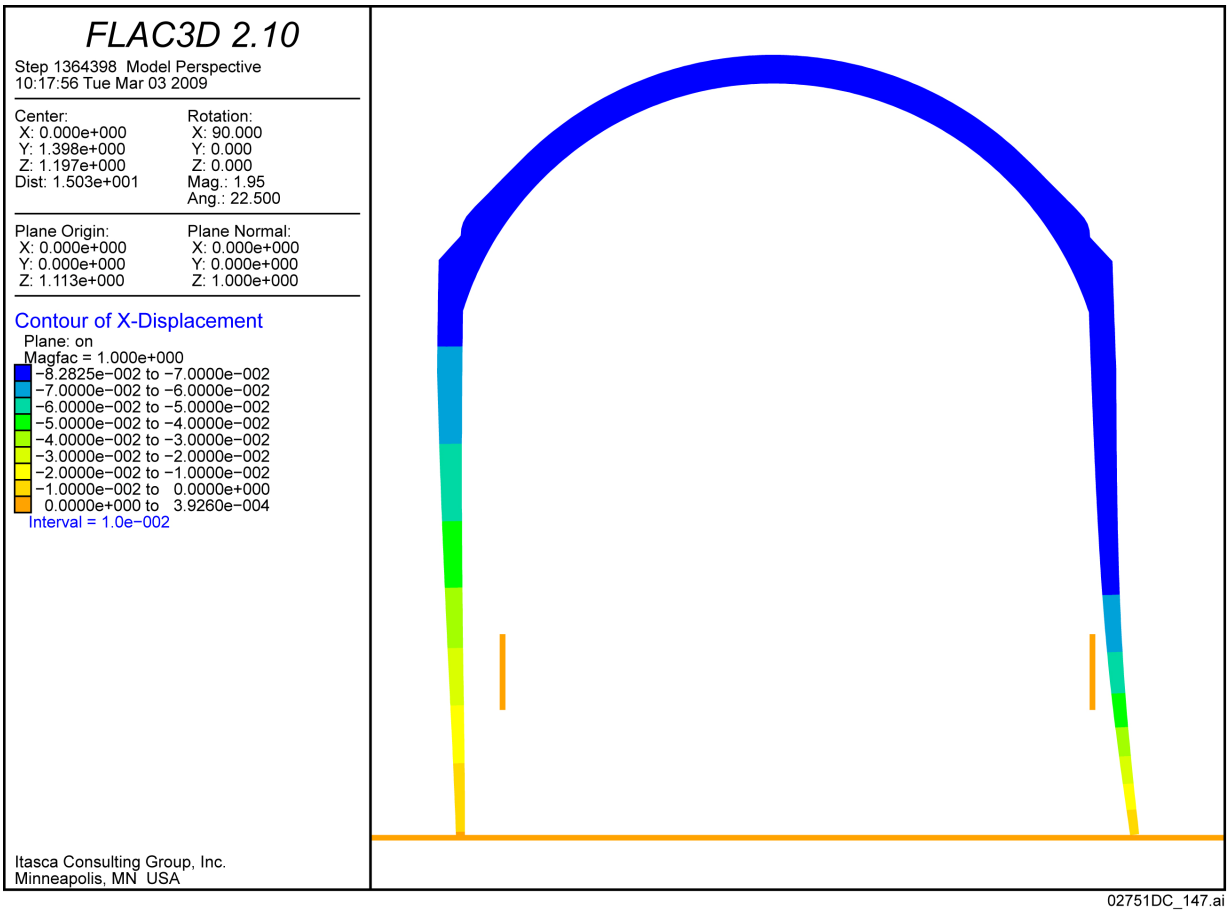

NOTE: Units are meters; positive displacements are to the right.

Figure 24. Realization 6: Drip Shield Configuration and Contours of Horizontal Displacements at State of Complete Drift Collapse Calculated in FLAC3D Model

2. COMMITMENTS TO NRC

None.

3. DESCRIPTION OF PROPOSED LA CHANGE

None.

4. REFERENCES

BSC (Bechtel SAIC Company) 2004a. *Drift Degradation Analysis*. ANL-EBS-MD-000027 REV 03. Las Vegas, Nevada: Bechtel SAIC Company. ACC: DOC.20040915.0010; DOC.20050419.0001; DOC.20051130.0002; DOC.20060731.0005; LLR.20080311.0066.

BSC 2004b. *Structural Stability of a Drip Shield Under Quasi-Static Pressure*. 000-00C-SSE0-00500-000-00A. Las Vegas, Nevada: Bechtel SAIC Company. ACC: ENG.20040830.0032; ENG.20080312.0017.

BSC 2005. *Creep Deformation of the Drip Shield*. CAL-WIS-AC-000004 REV 0A. Las Vegas, Nevada: Bechtel SAIC Company. ACC: DOC.20050830.0007.

SNL (Sandia National Laboratories) 2007. *Mechanical Assessment of Degraded Waste Packages and Drip Shields Subject to Vibratory Ground Motion*. MDL-WIS-AC-000001 REV 00. Las Vegas, Nevada: Sandia National Laboratories. ACC: DOC.20070917.0006; DOC.20080623.0002; DOC.20081021.0001.

RAI Volume 3, Chapter 2.2.1.3.2, Number 7:

Provide a technical basis to exclude temperature-dependent effects on titanium material properties used in the drip-shield mechanical analyses for 10,000 years following repository closure. Alternatively, demonstrate that temperatures expected for the drip shield during that time (i.e., greater than 60 °C [140 °F]) will not significantly affect the drip shield mechanical analyses.

Basis: The applicant's drip shield assessment used titanium material properties at 60 °C [140 °F] because, according to SAR Section 2.3.4.5.1.3.1, this temperature maximizes strain and deformation for 99 percent of the 1,000,000 year performance period. This assessment is based on analysis for an intact drift configuration, where the 60 °C [140 °F] temperature threshold would be exceeded during the first 10,000 years at the drift wall (SNL, 2007a; Figure 1-3). Temperatures higher than 60 °C [140 °F] would decrease the mechanical material properties of titanium materials (SAR Section 2.3.4.5.1.3.1; ASME, 2004), potentially decreasing the drip shield capacity. According to the applicant's results, drip shields may be subjected to static and dynamic loads during the first 10,000 years, when temperatures are greater than 60 °C [140 °F] (e.g., SAR Figure 2.1-14). Thus, the potential significance of temperature-dependent effects on titanium material properties must be addressed in the drip-shield mechanical analyses.

1. RESPONSE

During the first 650 years after repository closure, the fragility curves for buckling of the drip shield sidewalls and for rupture of the drip shield plates will be insensitive to changes in the temperature dependence of the mechanical properties of titanium because: (1) minimal rockfall is expected to accumulate in the drifts, (2) general corrosion does not have a significant effect on the thickness of the drip shield components, and (3) major seismic events with the potential to damage the drip shield occur very rarely during the first 650 years after closure. Between 650 years and 10,000 years after repository closure, 120°C provides an upper bound for drip shield temperature, and the associated changes in temperature-dependent mechanical properties between 60°C and 120°C for Titanium Grades 7 and 29 will have a minor impact on the fragility curves for plate rupture or sidewall buckling.

1.1 IN-DRIFT CONDITIONS

1.1.1 Drip Shield Temperature During the First 10,000 Years

The range of waste package temperatures for a drift with minimal rubble accumulation is shown in Figure 1. Minimal rubble accumulation is consistent with the expected volume of rockfall during the first 10,000 years after closure, as explained in Section 1.1.2 of this response.

The peak waste package temperature occurs within the first 100 years after repository closure and varies between 100°C and 210°C. The maximum waste package temperature decreases to 120°C at approximately 650 years after closure. A temperature of 120°C is then an upper bound for waste package temperature after 650 years for all thermal-hydrologic realizations in Figure 1.

The drip shield temperature will be less than the waste package temperature and greater than the drift wall temperature. There is a 10°C to 30°C difference between the waste package and drift wall temperatures during the peak of the thermal pulse (SNL 2008a, Table 6.3-49[a]). After 1,000 years, the waste package and drift wall temperatures are quite close, as shown by comparing the upper and lower plots in Figure 6.3-76[a] of *Multiscale Thermohydrologic Model* (SNL 2008a). It follows that the drip shield temperature is expected to be within a few degrees Celsius of the waste package temperature after the initial thermal pulse.

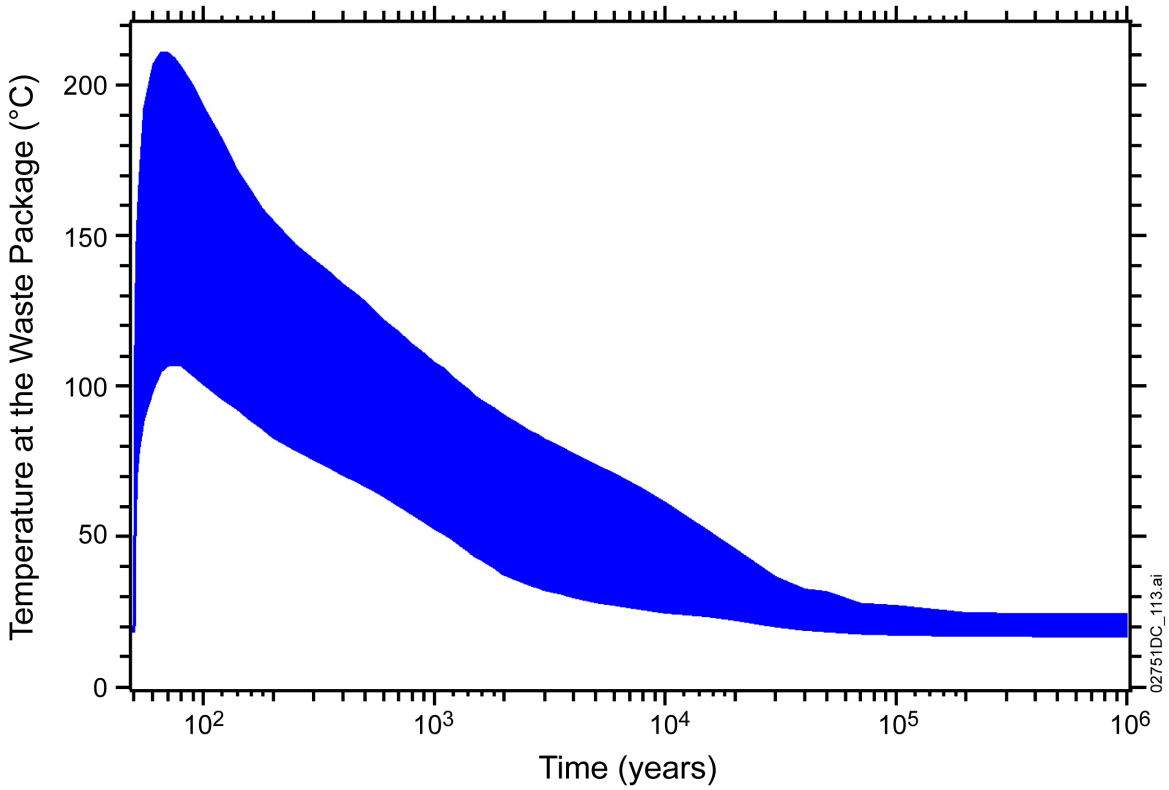

Source: SNL 2008a, Figure 6.3-76[a].

NOTE: The areas shown in blue represent "horsetail plots" of 182,784 waste package temperature histories, which is the product of eight waste package types, 3,264 locations across the repository, and seven uncertainty cases. The minimum and maximum values represent either a minimum or maximum value for all 182,784 histories at any point in time.

Figure 1. Range in Waste Package Temperature for the Range of Parametric Uncertainty Addressed in *Multiscale Thermohydrologic Model* (SNL 2008a)

The sensitivity of the drip shield fragility curves to the temperature dependence of the mechanical properties for titanium is evaluated in two parts: (i) during the first 650 years after repository closure, and (ii) between 650 years and 10,000 years after closure, when 120°C provides an upper bound for drip shield temperature.

1.1.2 Volume of Rockfall During the First 10,000 Years

Minimal rockfall accumulates in the repository during the first 10,000 years after repository closure. The mean rubble volume generated by seismic-induced rockfall is less than 0.2 m^3 per meter of drift length and 0.1 m^3 per meter of drift length for the lithophysal and nonlithophysal rock zones, respectively, for the first 650 years after repository closure (SAR Figure 2.1-6). The mean rubble volume generated by seismic-induced rockfall is less than 5 m^3 per meter of drift length and 0.5 m^3 per meter of drift length for the lithophysal and nonlithophysal rock zones, respectively, for the first 10,000 years after repository closure (SAR Section 2.1.2.1.6.2 and Figure 2.1-6). At 10,000 years, approximately 11% of realizations have lithophysal rockfall at or above 5 m^3 per meter of drift length, and only approximately 1% of the realizations have lithophysal rockfall exceeding 60 m^3 per meter of drift length (SNL 2008b, Section 7.3.2.6.1.3.4). The curves for the 5th percentile and median are absent from SAR Figure 2.1-6 because a large number of realizations have very little or no drift degradation from seismic events during the first 10,000 years after repository closure.

These rubble volumes can be compared to the volume between the sides of the drip shield and the drift walls to determine if the crown of the drip shield is covered with a significant amount of rubble. The diameter of the drift is 216 inches. The nominal widths of the drip shield at its base and shoulder are 99.8 inches and 89.48 inches, respectively. The average width is then (0.5)(99.8 + 89.48) = 94.64 inches. The shoulder height is 87.4 inches. The cross-sectional area between the sides of the drip shield and the drift walls can be estimated as (216 inches – 94.64 inches)(87.4 inches) = 10,607 in^2 = 73.7 ft^2 = 6.8 m^2. This is equivalent to a free volume between the sides and drift walls of 6.8 m^3 per meter of drift.[1] Even 10,000 years after repository closure, many realizations will have only minor rubble accumulation around the base of the drip shield, and the mean lithophysal rubble volume, which is less than 5 m^3 per meter of drift, contacts the sides the drip shield but does not cover the crown of the drip shield. Only 11% of the realizations during the first 10,000 years after repository closure have rockfall that exceeds 5 m^3 per meter of drift and have the possibility of covering the top of the drip shield.

1.2 TITANIUM MECHANICAL PROPERTIES AT 60°C AND 120°C

The analyses of drip shield fragility was conducted for a design in which the drip shield structural stiffeners are fabricated from Titanium Grade 24 (UNS R56405), the plates from Titanium Grade 7 (UNS R52400), and the base plates from Alloy 22. In a subsequent version of the drip shield design, the structural stiffeners were changed to Titanium Grade 29

[1] A more exact calculation with the curvature of the drift walls results in a free volume between sidewalls and drift walls of 6.4 m^3 per meter of drift (see Attachment B), as opposed to 6.8 m^3 from the simpler approach. This difference is minor because both values are greater than the mean rockfall volume of 5 m^3 per meter that is discussed later in this paragraph.

(UNS R56404). The original analyses are considered adequate because Grade 24 can be assumed to be analogous to Grade 29. Both alloys are based upon an extra-low-interstitial version of Titanium Grade 5 (Ti-6A1-4V) with the addition of a platinum group metal to improve corrosion performance. Microstructurally, there should be effectively no difference between Grades 24 and 29, as explained in Section 1.1 of the response to RAI 3.2.2.1.2.1-3-011. For the purposes of this response, the effect of temperature dependent material properties for Titanium Grades 24 or 29 on the structural response of the drip shield is considered to be equivalent.

The key mechanical properties for Titanium Grade 7 and Titanium Grade 24 at 60°C and 120°C are presented in Tables 1 and 2, respectively. Tables 1 and 2 also present the percent change in each mechanical property between 60°C and 120°C.

Table 1. Mechanical Properties of Titanium Grade 7 at 60°C and 120°C

Mechanical Property	60°C	120°C	% Change 60°C to 120°C
Modulus of Elasticity (MPa)	105,000	101,700	–3.1%
Yield Strength (MPa)	317	245	–23%
Ultimate Engineering Elongation (–)	0.247	0.319	+29%
Ultimate True Elongation (–)	0.221	0.277	+25%
Engineering Tensile Strength (MPa)	318	276	–13%
True Tensile Strength (MPa)	396	364	–8.1%
Tangent Modulus (MPa)	367	435	+18%

Source: Mechanical properties from Table A-1 in Attachment A of this response.

NOTE: Modulus of Elasticity is rounded to 4 significant digits and the other mechanical properties are rounded to three significant digits. Percent change rounded to two significant digits.

Table 2. Mechanical Properties of Titanium Grade 24 at 60°C and 120°C

Mechanical Property	60°C	120°C	% Change 60°C to 120°C
Modulus of Elasticity (MPa)	112,400	109,100	–2.9%
Yield Strength (MPa)	862	787	–8.6%
Ultimate Engineering Elongation (–)	0.178	0.175	–1.8%
Ultimate True Elongation (–)	0.164	0.161	–1.7%
Engineering Tensile Strength (MPa)	951	877	–7.9%
True Tensile Strength (MPa)	1,121	1,030	–8.1%
Tangent Modulus (MPa)	1,660	1,578	–4.9%

Source: Mechanical properties from Table A-2 of Attachment A of this response.

NOTE: Modulus of Elasticity is rounded to 4 significant digits and the other mechanical properties are rounded to three significant digits. Percent change rounded to two significant digits.

1.3 SENSITIVITY OF DRIP SHIELD FRAGILITY

1.3.1 During the First 650 Years After Repository Closure

During the first 650 years after repository closure, the fragility curves for buckling of the drip shield sidewalls and for rupture of the drip shield plates (SNL 2007b, Section 6.7) will be insensitive to changes in the temperature dependence of the mechanical properties of titanium because: (1) minimal rockfall is expected to accumulate in the drifts during the first 650 years after repository closure, (2) general corrosion does not have a significant effect on the thickness of the drip shield components during the first 650 years after closure, and (3) major seismic events with the potential to damage the drip shield occur very rarely during the first 650 years after closure.

The expected seismic-induced rockfall volumes that can accumulate during the first 650 years after repository closure are less than 0.2 m^3 per meter of drift. This volume represents a very small fraction of the free space on the sides of the drip shield, 6.8 m^3 per meter of drift (from Section 1.1.2 of this response). The accumulated rubble therefore provides minimal loading on the drip shield during the first 650 years after closure.

The potential for general corrosion to reduce the thickness of drip shield components is analyzed in Section 1.1.2 of the response to RAI 3.2.2.1.3.2-009. The estimated thickness reduction of the drip shield plates is about 2 mm over 10,000 years with a fourfold increase in mean corrosion rates. The estimated thickness reduction of the plates over 650 years is (2 mm)(650 years)/(10,000 years) = 0.13 mm, which is negligible compared to the initial plate thickness of 15 mm. The estimated thickness reduction of the interior bulkheads and longitudinal stiffeners on the underside of the plates is about 3 mm over 10,000 years, again with a fourfold increase in mean corrosion rates. The estimated thickness reduction of the framework components over 650 years is (3 mm)(650 years)/(10,000 years) = 0.195 mm, which is negligible compared to the initial thickness of the bulkheads or stiffeners in their minimum dimension, 38 mm. These calculations lead to the conclusion that the drip shield is essentially in its as-emplaced condition during the first 650 years after repository closure.

Localized corrosion could potentially initiate on external support beams on the sidewalls of the drip shield because these beams are fabricated from Titanium Grade 29. The response to RAI 3.2.2.1.3.2-009 supports the basis for excluding localized corrosion of the drip shield from total system performance assessment (TSPA), and it is not considered here.

Major seismic events are very unlikely during a short interval of time, such as the first 650 years after repository closure. Consider seismic events at the 1.05 m/s PGV level or greater. The hazard curve defines the exceedance frequency for seismic events between the 1 m/s and 4.07 m/s PGV levels as (10^{-5} per year – 10^{-8} per year) ≈ 10^{-5} per year (SNL 2007b, Section 6.4 and Table 6-3). Then the expected number of these seismic events over a 650 year period is (10^{-5} per year)(650 years) = 0.0065 (assuming a Poisson process of randomly occurring events, as is done in TSPA). Stated differently, on average there will be 6 to 7 aleatory realizations out of 1,000 aleatory realizations that have a seismic event greater than 1.05 m/s PGV level in TSPA during 650 years. So seismic events with a significant PGV level occur very rarely and, when

they do occur, the PGV levels around 1 m/s occur about 1,000 times more frequently than around the 4.07 m/s PGV level.

Collectively, these results indicate that the drip shield remains in its as-emplaced condition, there are minimal rockfall loads on the drip shield, and significant seismic events with the potential to damage the drip shield are very unlikely during the first 650 years after repository closure. Thus, the drip shield fragility, which is its probability of failure, remains zero or very close to zero for either buckling of the framework of rupture of the plates during the first 650 years after repository closure.

1.3.2 Sensitivity of Drip Shield Fragility to the Temperature Dependence of Titanium Material Properties between 650 Years to 10,000 Years after Repository Closure

Table 3 has the probability of rupture (i.e., the fragility) of the drip shield plates for two drift configurations: a drift that has no rubble and a drift that is 10% filled with rubble (SNL 2007b, Section 6.8). The small rubble loads are consistent with minimal rubble accumulation in the drifts during the first 10,000 years after repository closure, as explained in Section 1.1.2. Although the data in Table 3 are based on structural response calculations for mechanical properties at 60°C, the dependence of fragility on plate thickness provides information that is useful for estimating the sensitivity of fragility to temperature-dependent material properties.

Table 3 demonstrates that a reduction in plate thickness from 15-mm, its initial thickness, down to 2-mm has no significant impact on the probability of rupture. Since a thickness reduction of (13 mm)/(15 mm) = 86.6% has no significant impact on fragility, the potential changes in mechanical properties from 60°C to 120°C, as shown in Table 1, should not have a significant impact on the plate fragility calculations. More specifically, a thickness reduction of 86.6% will produce significant changes in stress and strain in the plates for a given load. The material properties in Table 1 show differences between +18% to –23%, which will also change stress and strain for a given load. (The percent changes from Table 1 exclude the +25% and +29% changes for elongation, which are beneficial because the material is becoming more ductile at elevated temperature.) The percent changes in material properties are a factor of 3 to 4 less than the percent thickness reduction, leading to the conclusion that the temperature dependence of mechanical properties between 60°C and 120°C for Titanium Grade 7 will have a minor impact on the fragility curves for plate rupture.

Table 4 provides similar information for the probability of buckling of the drip shield framework. The small rubble loads are consistent with minimal rubble accumulation in the drifts during the first 10,000 years after repository closure (see Section 1.1.2). The data in Table 4 are again based on structural response calculations for mechanical properties at 60°C, and assume uniform thinning of all drip shield components. With a 10% rockfall load, Table 4 demonstrates that a reduction in component thickness by 5 mm and 10 mm has no significant impact on the probability of buckling. Since the initial minimum thickness of the bulkheads and stiffeners that provide the framework beneath the plates is 38 mm, a thickness reduction of (10 mm)/(38 mm) = 26% has no impact on the fragility data in Table 4. A thickness reduction of 26% will produce changes in the stress and strain distributions in the drip shield structural support for a given load.

Table 3. Probability of Plate Rupture for the Drip Shield Plates

PGV Level (m/s)	Plate Thickness				
	0 mm	**2 mm**	**5 mm**	**10 mm**	**15 mm**
Probability of Failure with 0% Rockfall Load:					
All	1	0	0	0	0
Probability of Failure with 10% Rockfall Load:					
0.2	1	0	0	0	0
0.4	1	0	0	0	0
1.05	1	0	0	0	0
2.44	1	0.006	0	0	0
4.07	1	0.036	0	0	0

Source: SNL 2007b, Table 6-36.

NOTE: Probabilities below 0.001 have been rounded down to 0.

Table 4. Probability of Sidewall Buckling for the Drip Shield Framework

PGV Level (m/s)	Thicknesses of Drip Shield Components				
	Frame: Reduced by 15 mm	**Frame: Reduced by 13 mm**	**Frame: Reduced by 10 mm**	**Frame: Reduced by 5 mm**	**Frame: Intact**
Probability of Failure with 0% Rockfall Load:					
All	1	0	0	0	0
Probability of Failure with 10% Rockfall Load:					
0.2	1	0	0	0	0
0.4	1	0	0	0	0
1.05	1	0.007	0	0	0
2.44	1	0.107	0.001	0	0
4.07	1	0.311	0.011	0	0

Source: SNL 2007b, Table 6-40.

NOTE: Probabilities below 0.001 have been rounded down to 0.

The analysis of drip shield framework fragility was conducted for a design in which the drip shield structural stiffeners are fabricated from Titanium Grade 24 (UNS R56405), the plates from Titanium Grade 7 (UNS R52400), and the base plates from Alloy 22. In a subsequent version of the drip shield design, the structural stiffeners were changed to Titanium Grade 29 (UNS R56404). The original analyses are considered adequate because Grade 24 can be assumed to be analogous to Grade 29. Both alloys are based upon an extra-low-interstitial version of Titanium Grade 5 (Ti-6A1-4V) with the addition of a platinum group metal to improve corrosion performance. Microstructurally, there should be effectively no difference between Grades 24 and 29, as explained in Section 1.1 of the response to RAI 3.2.2.1.2.1-3-011. For the purposes of this response, the effect of temperature dependent material properties for Titanium Grades 24 or 29 on the structural response of the drip shield framework is considered to be equivalent.

Table 2 shows that the potential changes in mechanical properties for Titanium Grade 24 from 60°C to 120°C are −1.7% to −8.6%, which will produce minor changes in stress and strain for a given load. The percent change of −8.6% in material properties for Grade 24 is again a factor of 3 to 4 less than the percent thickness reduction, leading to the conclusion that the temperature dependence of mechanical properties between 60°C and 120°C for Titanium Grade 24 or Grade 29 will have at most a minor impact on the fragility curves for buckling of the sidewalls.

1.4 CONSISTENCY WITH RELATED FEPS

This analysis demonstrates that drip shield response is insensitive to temperature-dependent mechanical properties during the first 10,000 years after repository closure. Given this insensitivity, the results in this response have no relevance to excluded FEPs 2.1.03.03.0B, Localized Corrosion of Drip Shields; 2.1.06.05.0B, Mechanical Degradation of Invert; and 2.1.07.06.0A, Floor Buckling. These results are not relevant to excluded FEP 2.1.07.05.0B, Creep of Metallic Materials in the Drip Shield, because creep properties were evaluated at 150°C for the exclusion justification.

1.5 CONCLUSION

This analysis demonstrates that drip shield temperatures, which can be greater than 60°C (140°F) during the first 10,000 years after repository closure, will not significantly affect the mechanical response of the drip shield. During the first 650 years after repository closure, the fragility curves for buckling of the drip shield sidewalls and for rupture of the drip shield plates will be insensitive to changes in the temperature dependence of the mechanical properties of titanium because: (1) minimal rockfall is expected to accumulate in the drifts, (2) general corrosion does not have a significant effect on the thickness of the drip shield components, and (3) major seismic events with the potential to damage the drip shield occur very rarely during the first 650 years after closure. Between 650 years and 10,000 years after repository closure, 120°C provides an upper bound for drip shield temperature. The changes for temperature dependent mechanical properties between 60°C and 120°C for Titanium Grades 7 and 29 will have a minor impact on the fragility curves for plate rupture or sidewall buckling because the percent changes in the titanium mechanical properties between 60°C and 120°C are a factor of 3 to 4 less than the corresponding percent changes in component thicknesses that have no impact on with the fragility values.

2. COMMITMENTS TO NRC

None.

3. DESCRIPTION OF PROPOSED LA CHANGE

None.

4. REFERENCES

SNL (Sandia National Laboratories) 2007a. *Mechanical Assessment of Degraded Waste Packages and Drip Shields Subject to Vibratory Ground Motion*. MDL-WIS-AC-000001 REV 00. Las Vegas, Nevada: Sandia National Laboratories. ACC: DOC.20070917.0006.

SNL 2007b. *Seismic Consequence Abstraction*. MDL-WIS-PA-000003 REV 03. Las Vegas, Nevada: Sandia National Laboratories. ACC: DOC.20070928.0011.

SNL 2008a. *Multiscale Thermohydrologic Model*. ANL-EBS-MD-000049 REV 03. Las Vegas, Nevada: Sandia National Laboratories. ACC: DOC.20080201.0003.

SNL 2008b. *Total System Performance Assessment Model-Analysis for the License Application*. MDL-WIS-PA-000005 REV 00 ADD 01. Las Vegas, Nevada: Sandia National Laboratories. ACC: DOC.20080312.0001.

5. LIST OF ATTACHMENTS

Attachment A: CALCULATION OF MECHANICAL PROPERTIES FOR TITANIUM GRADE 7 AND TITANIUM GRADE 24 AT 120°C

Attachment B: EXACT CALCULATION OF FREE VOLUME BETWEEN THE DRIP SHIELD SIDEWALLS AND THE CIRCULAR DRIFT WALLS

ATTACHMENT A

CALCULATION OF MECHANICAL PROPERTIES FOR TITANIUM GRADE 7 AND TITANIUM GRADE 24 AT 120°C

Tables A-1 and A-2 summarize the calculations for mechanical properties at 60°C and 120°C for Titanium Grades 7 and 24. The input data in Tables A-1 and A-2 are at 21°C, 93°C, 204°C, and 232°C. The computational methods are identical with the approach documented in *Mechanical Assessment of Degraded Waste Packages and Drip Shields Subject to Vibratory Ground Motion* (SNL 2007a, Appendix A): Young's modulus, yield strength, ultimate engineering elongation, and engineering tensile strength are linearly interpolated from measurements; ultimate true elongation, true tensile strength, and the tangent modulus are calculated by formula.

Table A-1. Mechanical Properties of Titanium Grade 7 (UNS R52400) at 60°C and 120°C

Mechanical Property	Temperature (°C)					Source
	21°C	60°C	93°C	120°C	204°C	
Young's Modulus, E	106,870	105,001 (interp)	103,420	101,744 (interp)	96530	
Yield Strength, σ_y	363	317 (interp)	N/A	245 (interp)	145	
Ultimate Engineering Elongation, e_u	0.2	0.247 (interp)	N/A	0.319 (interp)	0.42	
Ultimate True Elongation, ε_u	N/A	0.221 (formula)	N/A	0.277 (formula)	N/A	$\varepsilon_u = \ln(1 + e_u)$
Engineering Tensile Strength, s_u	345	318 (interp)	N/A	276 (interp)	218	
True Tensile Strength, σ_u	N/A	396 (formula)	N/A	364 (formula)	N/A	$\sigma_u = s_u(1 + e_u)$
Tangent Modulus, E_t	N/A	367 (formula)	N/A	435 (formula)	N/A	$E_t \equiv \frac{(\sigma_u - \sigma_y)}{(\varepsilon_u - \sigma_y/E)}$

Source: Data from SNL 2007a, Table A-1. Computational methodology is identical to this source.

NOTES: Properties are in the units of MPa except for elongation, which is unitless.

N/A = not applicable; (interp) = linear interpolation between nearest data points; (formula) = calculation by formula in the rightmost column.

Table A-2. Mechanical Properties of Titanium Grade 24 (UNS R56405) at 60°C and 120°C

Mechanical Property	Temperature (°C)					Source
	21°C	60°C	120°C	204°C	232°C	
Young's Modulus, E	114,500	112,374 (interp)	109,104 (interp)		103,000	
Yield Strength, σ_y	910	862 (interp)	787 (interp)	683	N/A	
Ultimate Engineering Elongation, e_u	0.18	0.178 (interp)	0.175 (interp)	0.17	N/A	
Ultimate True Elongation, ε_u	N/A	0.164 (formula)	0.161 (formula)	N/A	N/A	$\varepsilon_u = \ln(1 + e_u)$,
Engineering Tensile Strength, s_u	1,000	951 (interp)	877 (interp)	772	N/A	
True Tensile Strength, σ_u	N/A	1,121 (formula)	1,030 (formula)	N/A	N/A	$\sigma_u = s_u(1 + e_u)$
Tangent Modulus, E_t	N/A	1,660 (formula)	1,578 (formula)	N/A	N/A	$E_t \equiv \frac{(\sigma_u - \sigma_y)}{(\varepsilon_u - \sigma_y/E)}$

Source: Data from SNL 2007a, Table A-2. Computational methodology is identical to this source.

NOTES: Properties are in the units of MPa except for elongation, which is unitless.

N/A = not applicable; (interp) = linear interpolation between nearest data points; (formula) = calculation by formula in the rightmost column.

ATTACHMENT B

EXACT CALCULATION OF FREE VOLUME BETWEEN THE DRIP SHIELD SIDEWALLS AND THE CIRCULAR DRIFT WALLS

An exact calculation of the free volume between the sidewalls of the drip shield (DS) and the circular drift walls is based on the following equation:

$$\text{Free Area} = (\text{Area of Drift}) - (\text{Area of Invert}) - (\text{Area Above DS Shoulder}) - (\text{DS area}) \qquad \text{(Eq. B-1)}$$

The area of the invert and the area above the shoulder of the drip shield are based on the area of a sector of a circle and include the effect of the curved walls of the drip shield.

Area of the drift

The diameter of the drift cross-section is 216 inches (SNL 2007b, Figure 6-107), so the drift radius is 108 inches. The area of the drift is then $\pi(108 \text{ inches})^2 = 36{,}644 \text{ in}^2$.

Area of the invert

The invert is 52 inches high at its center (SNL 2007b, Figure 6-107), so the top of the invert is (108 in − 52 in) = 56 in from the center of the drift cross-section. The central half-angle subtended by the top of the invert is then given by $\cos^{-1}(56/108) = 58.767$ degrees. The area of the circular sector containing the full invert is then $(2*58.767^{\circ}/360^{\circ})\pi(108 \text{ in})^2 = 11{,}964 \text{ in}^2$. The triangular area formed by the extreme end points of the invert and the center of the circle is given by: $(56)(108)\sin(58.767°) = 5{,}171 \text{ in}^2$. The cross-sectional area of the invert is then $11{,}964 \text{ in}^2 - 5{,}171 \text{ in}^2 = 6{,}793 \text{ in}^2$.

Area Above the Shoulder of the Drip Shield

The height of the shoulder of the drip shield is 87.4 in. The top of the shoulder is then (52 in + 87.4 in) = 139.4 in above the lowest point of the drift floor, or (139.4 in – 108 in) = 31.4 in above the center of the drift cross-section. The central half-angle subtended by a horizontal line through the shoulder of the drip shield is then given by $\cos^{-1}(31.4/108) = 73.098$ degrees. The area of the circular sector containing the horizontal line through the shoulder is then $(2*73.098^{\circ}/360°)\pi(108 \text{ in})^2 = 14{,}881 \text{ in}^2$. The triangular area formed by the end points where the horizontal line meets the circle and the center of the circle is given by: $(31.4)(108)\sin(73.098°) = 3{,}244.7 \text{ in}^2$. The cross-sectional area of the circular sector bounded by the horizontal line through the shoulder and the drift wall is then $14{,}881 \text{ in}^2 - 3{,}244.7 \text{ in}^2 = 11{,}636.3 \text{ in}^2$.

Cross-Sectional Area of the Drip Shield

The cross-sectional area of the drip shield is based on the product of the average width of the sidewalls, 94.64 inches (see Section 1.1.2 of this response), and the shoulder height of the drip shield, 87.4 inches: $(94.64 \text{ in})(87.4 \text{ in}) = 8{,}271.5 \text{ in}^2$.

Calculation of Free Area and Free Volume from Equation B-1

$$\text{Free Area} = (36{,}644\ \text{in}^2) - (6{,}793\ \text{in}^2) - (11{,}636.3\ \text{in}^2) - (8{,}271.5\ \text{in}^2),$$
$$= 9{,}943.2\ \text{in}^2\ (69.05\ \text{ft}^2 \text{ or } 6.4\ \text{m}^2).$$

The corresponding volume between the sidewalls and the drift walls is then 6.4 m^3 per meter of drift length.

RAI Volume 3, Chapter 2.2.1.3.2, Number 8:

Provide a technical basis to support use of the FLAC3D code to represent linear and nonlinear response in the structural analyses. Also provide the input parameters and model assumptions for the alternative structural analysis code that was used in developing support for the FLAC3D methodology (SNL 2007; Section 7.3.3).

Basis: The applicant's assessment was based on an adaptation of a geotechnical engineering analysis code (FLAC3D) for use in structural analysis. However, conventional input parameters for nonlinear performance evaluation of metal components cannot be directly implemented in FLAC3D (SNL 2007; Table 6-134). For example, the strain hardening is formulated in terms of the dependence of cohesion on plastic shear strain (SNL 2007; Section 6.4.2). To support the use of FLAC3D models, the applicant compared deformed shapes and maximum shear stress contours with results obtained using an alternative structural analysis code (SNL 2007; Section 7.3.3). This comparison, however, presents limited information on the technical basis for input parameters, important model assumptions, and stress and strain distributions. Moreover, the drip shield response for the evaluated cases appears to be mostly in the linear range of the materials, where the nonlinear parameters cannot be tested. Thus, a comprehensive evaluation is needed to show that FLAC3D models provide a reasonable structural response at the expected system performance levels.

1. RESPONSE

1.1 INTRODUCTION

FLAC3D is a numerical code appropriate for use in analysis of linear and nonlinear response in the structural analysis. The code has been widely used, tested, and validated for solution of problems that include significant geometrical and material nonlinearities. In the analysis of drip shield response and load bearing capacity, the Tresca constitutive relation with zero plastic volumetric strain, which is commonly used for representation of metals, is used as material model for titanium. In this response, it is demonstrated on a simple one-dimensional problem that FLAC3D matches idealized stress-strain and volumetric response of titanium.

The drip shield analyses in *Mechanical Assessment of Degraded Waste Packages and Drip Shields Subject to Vibratory Ground Motion* (SNL 2007) were conducted using the numerical code FLAC3D (Fast Lagrangian Analysis of Continua in 3 Dimensions). FLAC3D is a general purpose three-dimensional, explicit finite-difference program for engineering mechanics computation. Although FLAC3D is widely used for analysis and simulation of problems in geotechnical engineering, its formulation is completely general and can be applied to analysis of elastic and inelastic deformation of structures made of different materials, provided that appropriate constitutive relationships are used.

1.2 TECHNICAL BASIS

Application of FLAC3D to structural analysis of the drip shield is within the range of its validation. There was no need to adapt the code for doing structural analysis of the drip shield. Tresca yield criterion, which is a constitutive relation typically used for representation of metals, was used in the FLAC3D drip shield simulations to represent Titanium Grade 7 and Titanium Grade 24 (e.g., Popov 1968, pp. 316 to 319). The impact of using Titanium Grade 24 in the analysis instead of Titanium Grade 29 is discussed in Section 1.1 of the response to RAI 3.2.2.1.2.1-3-011. The Tresca yield criterion is a special case of the Mohr-Coulomb yield criterion when the friction angle is zero. FLAC3D is extensively used and validated for the Mohr-Coulomb yield criterion.

The input parameters, which are used in the FLAC3D simulations to characterize mechanical behavior of titanium, are equivalent to the conventional input parameters and can be calculated from the conventional input parameters using simple and standard solid mechanics formulas. For example, FLAC3D uses bulk, K, and shear, G, moduli as input elastic parameters, which can be calculated from more commonly used elastic parameters such as Young's modulus, E, and Poisson's ratio, ν, using the following basic relations (Jaeger and Cook 1979, Equations 13 and 14):

$$G = \frac{E}{2(1+\nu)} \qquad K = \frac{E}{3(1-2\nu)} \qquad \text{(Eq. 1)}$$

The cohesion, c_y, which is a parameter used to specify onset of yielding in FLAC3D, is calculated, knowing that the friction angle is zero, from the yield strength, σ_y, as follows:

$$c_y = \frac{\sigma_y}{2} \qquad \text{(Eq. 2)}$$

The post-yield strength increase is conventionally specified in terms of the tangent (hardening) modulus, E_t, which is a rate of increase in strength with respect to strain. Using the tangent modulus implies simple bi-linear material stress-strain response as shown in Figure 1. Bi-linear idealization of stress-strain response of metals is typically used in numerical analyses (SNL 2007, Section 4.1.2.1). FLAC3D allows more general post-yield response by allowing the user to specify a stress-strain response in a tabular form. The table contains pairs of plastic strain and cohesion values (i.e., points) starting with the yielding point (for which the plastic strain is zero). To represent the bi-linear stress-strain response (illustrated in Figure 1), it is sufficient to provide only two pairs (points) in the table, which correspond to desired yield strength and tangent modulus—i.e., the post-yield slope of the stress-strain curve.

Because only slope needs to be represented, the value of strain for the second point is arbitrary. If the second point corresponds to ultimate strain, ε_u, the corresponding plastic strain, ε_{up}, is calculated by subtracting the elastic strain:

$$\varepsilon_{up} = \varepsilon_u - \frac{\sigma_u}{E} \qquad \text{(Eq. 3)}$$

where σ_u is the ultimate stress related to tangent modulus by the following relation:

$$\sigma_u = \sigma_y + \left(\varepsilon_u - \frac{\sigma_y}{E} \right) E_t \qquad \text{(Eq. 4)}$$

Finally, the cohesion corresponding to the ultimate strength is:

$$c_u = \frac{\sigma_u}{2} \qquad \text{(Eq. 5)}$$

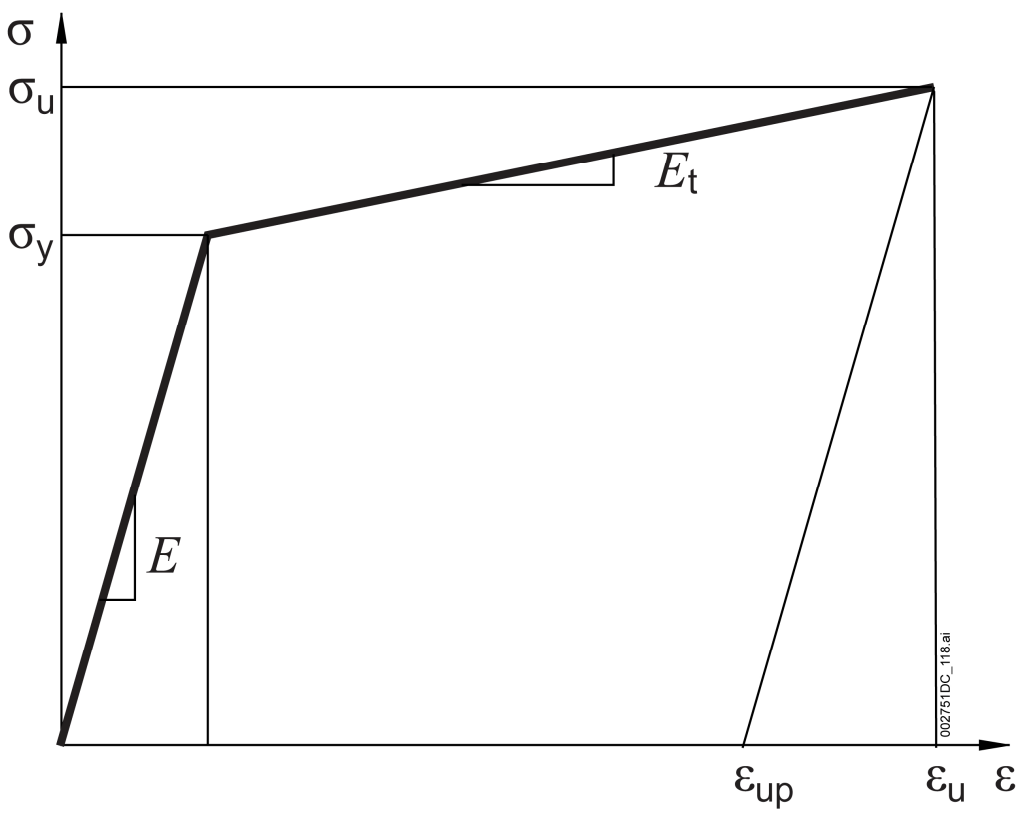

Figure 1. Bi-Linear Stress-Strain Curve

To demonstrate that irrespective of the choice of input parameters the representative stress-strain curves for Titanium Grade 7 and Titanium Grade 24 are obtained and that FLAC3D correctly simulates elastic and inelastic deformation of metals, simple numerical tests were carried out in FLAC3D. A single FLAC3D zone with properties of Titanium Grade 7 and Titanium Grade 24, listed in *Mechanical Assessment of Degraded Waste Packages and Drip Shields Subject to Vibratory Ground Motion* (SNL 2007, Table 6-134), is subjected to quasi-static one-dimensional tension. The bottom of the model was fixed in the vertical direction; a small, constant velocity is specified at the top of the model in the vertical direction. Since the zone has unit height, the displacements of the top are equal to strain. The simulation is carried out until strain of 0.1 is reached. The generated curves of vertical stress as functions of vertical (axial) strain are shown in Figures 2 and 3 for Titanium Grade 7 and Titanium Grade 24, respectively. The characteristic points and the slopes of the sections of the curves (i.e., the conventional parameters) are calculated from the generated data and included on the figures. If those parameters are compared with input parameters for Titanium Grade 7 and Titanium Grade 24 at 60°C as listed in *Mechanical Assessment of Degraded Waste Packages and Drip Shields Subject to Vibratory Ground Motion* (SNL 2007, Tables A-1 and A-2), it is clear that input parameters used in FLAC3D calculations are equivalent with conventional input parameters (namely the yield strength, Young's modulus, and the tangent modulus). Small disagreements (less than 1%) are a consequence of rounding during calculation of the parameters.

Unlike rocks and concrete, metals typically yield at constant volume—i.e., they do not dilate during shear. In the calculations, Titanium Grade 7 and Titanium Grade 24 are represented as Tresca materials with zero friction angle and zero dilation angle. Thus, the constitutive relations in FLAC3D numerical simulations correctly represent plastic deformation of titanium. Figure 4, which is obtained from FLAC3D simulation of a one-dimensional tension test on Titanium Grade 7 represented as Tresca material, confirms that volumetric strain is zero. The figure shows total and plastic volumetric strains as functions of axial strain. (The plastic volumetric strain is calculated subtracting the elastic volumetric strain, $\varepsilon_{ve} = \frac{\sigma}{E}(1-2\nu)$, from the total volumetric strain.) Clearly, the plastic volumetric strain is practically zero throughout the simulation. (The onset of plastic deformation is indicated by the change in slope in the curve of total strain.)

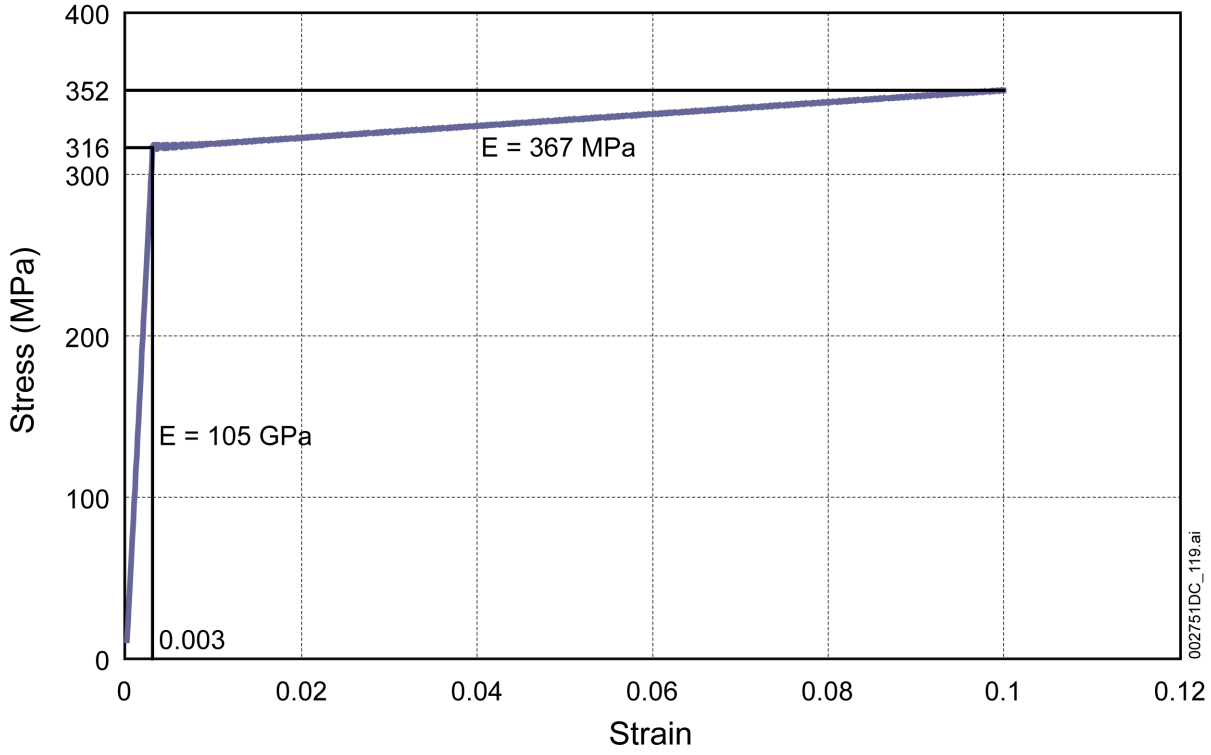

Figure 2. Stress-Strain Curve of Titanium Grade 7 as Represented in FLAC3D Model

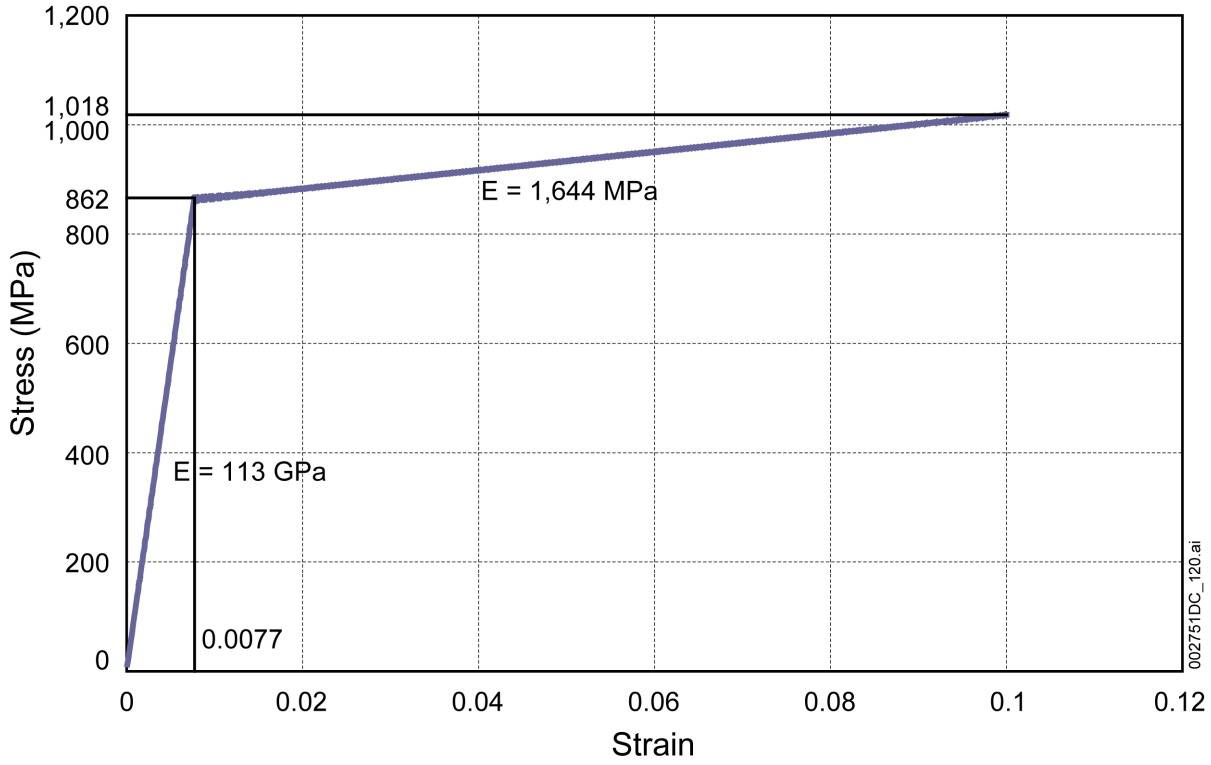

Figure 3. Stress-Strain Curve of Titanium Grade 24 as Represented in FLAC3D Model

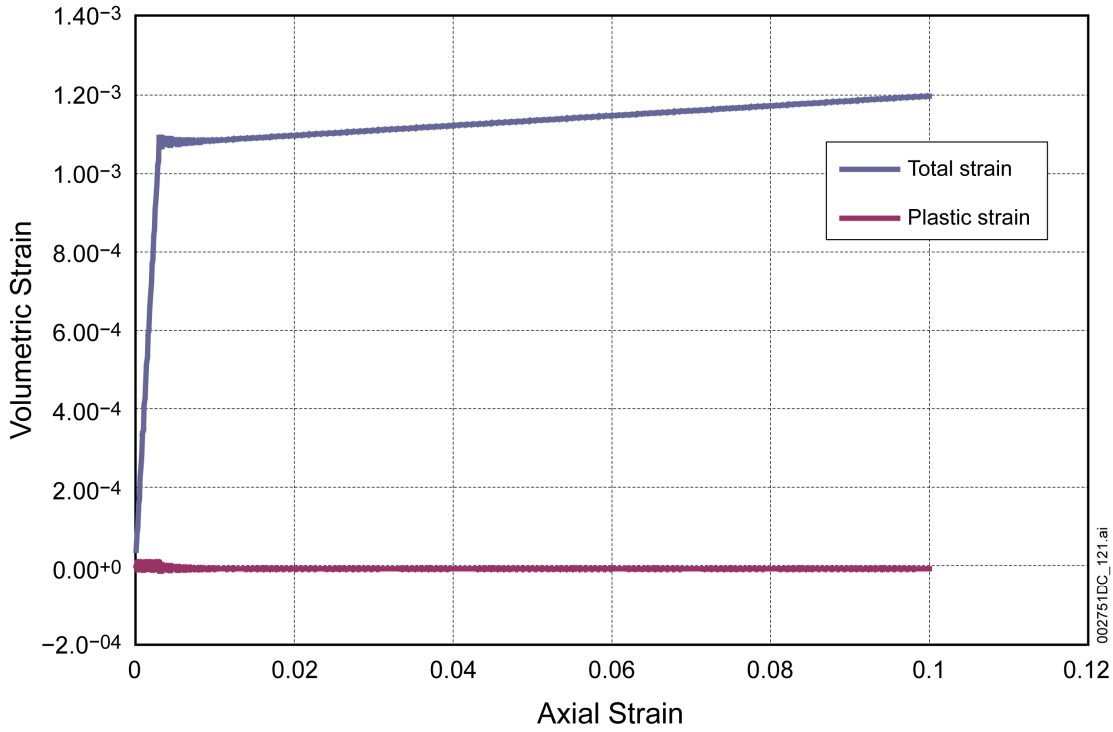

Figure 4. Total and Plastic Volumetric Strain Versus Axial Strain for Titanium Grade 7 as Represented in FLAC3D Model

1.3 INPUT PARAMETERS AND MODEL ASSUMPTIONS

The results of calculations of drip shield deformation and stresses due to six static rubble load realizations (SNL 2007, Table 6-136) obtained using FLAC3D and LS-DYNA are compared in *Mechanical Assessment of Degraded Waste Packages and Drip Shields Subject to Vibratory Ground Motion* (SNL 2007, Section 7.3.3.1). LS-DYNA (e.g., V960.1106, STN: 10300-960.1106-00) is a general purpose, solid mechanics finite element numerical code for analysis of elastic and inelastic deformation of solid bodies under static and dynamic loading conditions. The objective of the comparison was to provide additional validation of the FLAC3D drip shield model. As indicated in the drip shield perspective view in Figure 5, which shows areas of inelastic deformation for realization 3 (one of the six rubble load realizations with largest vertical pressure; SNL 2007, Table 6-136) of the static rubble load, the structural response for this load includes both elastic and inelastic deformation.

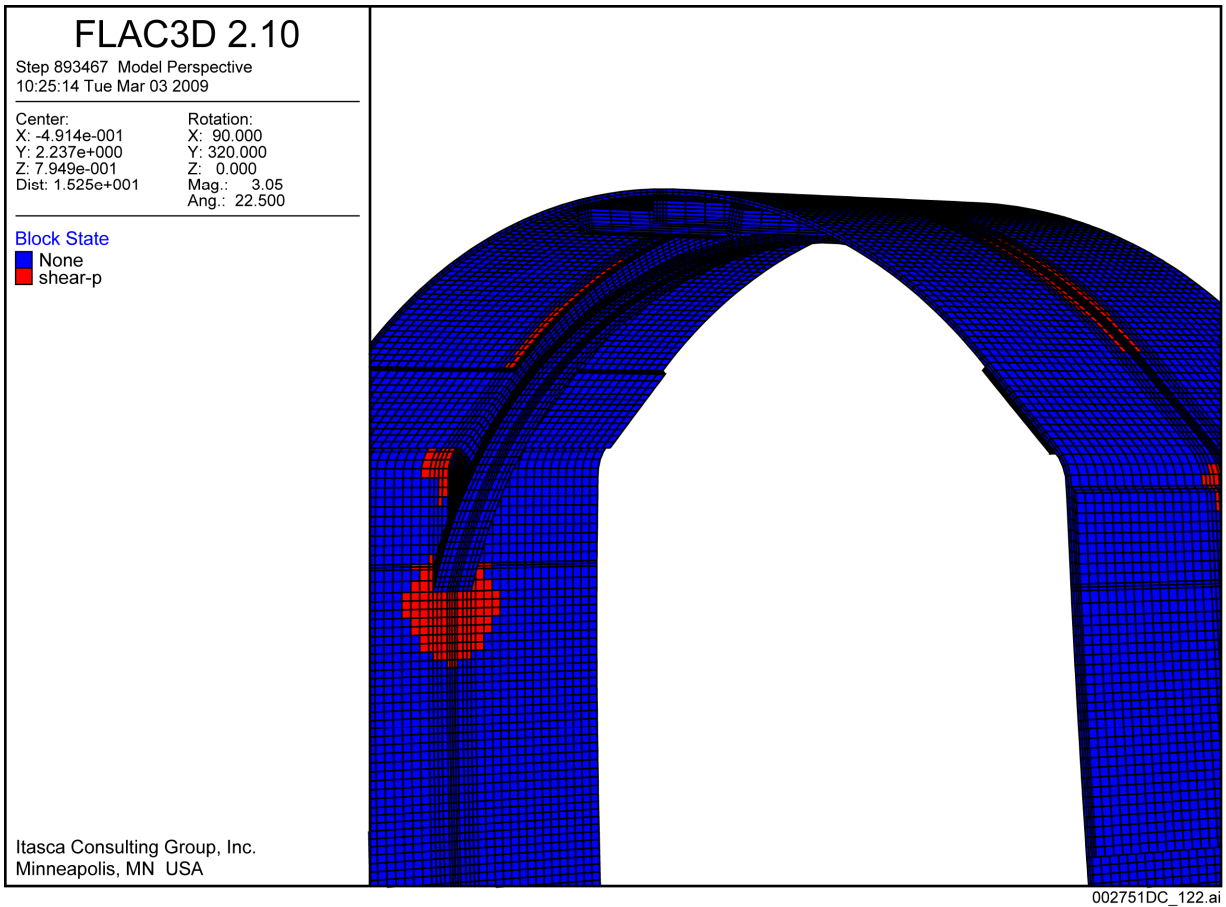

002751DC_122.ai

NOTE: The areas of inelastic deformation are red.

Figure 5. Indicators of Inelastic Deformation for Realization 3 of Static Rubble Load

The calculations were carried out to assess drip shield stability and structural integrity under static rubble load in the case of complete drift collapse. The details of the calculation, the input data and the assumptions are provided in *Structural Stability of a Drip Shield Under Quasi-Static Pressure* (BSC 2004). The following are the main assumptions used in both (LS-DYNA and FLAC3D) calculations:

- The sliding friction coefficient for the contact between the drip shield and the invert is 0.4.
- The temperature of the drip shield is assumed to be 150°C. The mechanical properties as calculated for 150°C were used in the calculation.
- The thickness of the Titanium Grade 7 and Titanium Grade 24 plates are reduced by 2 mm due to uniform corrosion (BSC 2004, Assumption 3.8).
- With exception of the lateral constraint provided by the emplacement pallet, the drip shield sides are assumed to be unconstrained in the lateral direction.

Geometry of both LS-DYNA and FLAC3D representations (which are identical) is shown in Figure 6. The mechanical properties of titanium at 150°C, as used in the LS-DYNA calculations are listed in Table 1. Similarly, the elastic properties used in the FLAC3D calculations are identical with those listed in Table 1. Comparison of the values for yield strength from the FLAC3D calculations (BSC 2005, Table 5.2-1) with yield strength values used in the LSDYNA calculations (Table 1 of this response) shows that the yield value for Titanium Grade 24 in Table 5.2-1 of *Creep Deformation of the Drip Shield* (BSC 2005) is about 9% less than the value in Table 1. For Titanium Grade 7, a similar comparison shows that the value in Table 5.2-1 is about 16% less than the value in Table 1 of the response. These differences in yield strength are relatively small and acceptable for purposes of model comparison.

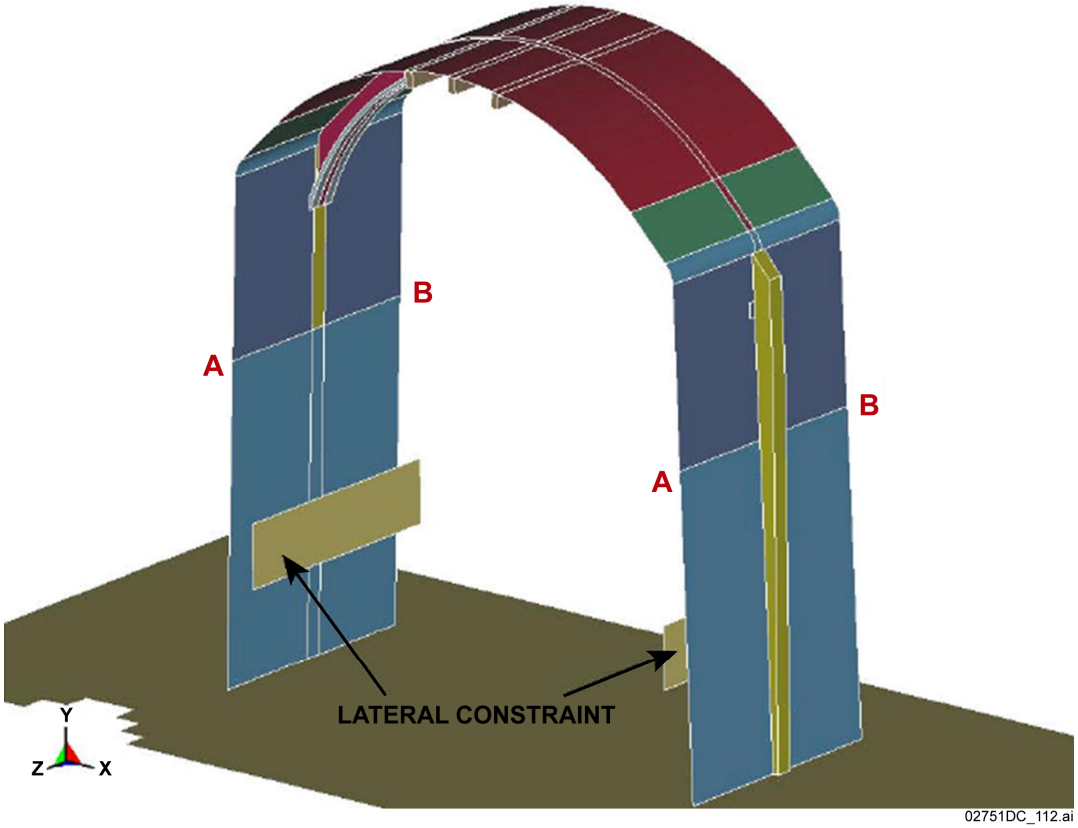

Source: BSC 2004, Figure 2.

Figure 6. Geometry of the Drip Shield Representations in LS-DYNA and FLAC3D Calculations

Table 1. Titanium Mechanical Properties Used in LS-DYNA Calculations

Mechanical Property	Titanium Grade 7	Titanium Grade 24
Density (kg/m^3)*	4,520	4,430
Yield strength (MPa)	209	750
Poisson's ratio*	0.32	0.34
Modulus of elasticity (GPa)	101	108
Tangent (hardening) modulus (GPa)	0.448	1.52

Source: BSC 2004, Section 5.1.

* Room temperatures used. All properties not marked with * are for 150°C.

1.4 CONSISTENCY WITH RELATED FEPS

FLAC3D is a numerical code appropriate for use in analysis of linear and nonlinear response in the structural analysis and, in particular, the analysis of the drip shield structural response. Use of this code is not relevant to the screening justifications for excluded FEPs 2.1.07.05.0B, Creep of Metallic Materials in the Drip Shield; 2.1.03.03.0B, Localized Corrosion of the Drip Shield; 2.1.06.05.0B, Mechanical Degradation of Invert; and 2.1.07.06.0A, Floor Buckling.

1.5 SUMMARY

FLAC3D is an appropriate numerical code for use in analysis of linear and nonlinear response in the structural analysis. FLAC3D is a general purpose solid mechanics code widely tested and validated on problems with significant geometrical and material nonlinearities. Its applicability to analysis of different materials depends on how accurately the constitutive relationships represent the material of interest. FLAC3D is extensively used and validated for use of the Mohr-Coulomb constitutive relation. The Tresca relation, which is the special case of the Mohr-Coulomb relation for friction angle set to zero, is appropriate and commonly used constitutive relation for representation of deformation and yielding of metals, including titanium. It is demonstrated that, for FLAC3D input parameters used in the drip shield simulation, the model accurately represents the specified stress-strain and volumetric response of Titanium Grade 7 and Titanium Grade 24.

2. COMMITMENTS TO NRC

None.

3. DESCRIPTION OF PROPOSED LA CHANGE

None.

4. REFERENCES

BSC (Bechtel SAIC Company) 2004. *Structural Stability of a Drip Shield Under Quasi-Static Pressure*. 000-00C-SSE0-00500-000-00A. Las Vegas, Nevada: Bechtel SAIC Company. ACC: ENG.20040830.0032; ENG.20080312.0017.

BSC 2005. *Creep Deformation of the Drip Shield*. CAL-WIS-AC-000004 REV 0A. Las Vegas, Nevada: Bechtel SAIC Company. ACC: DOC.20050830.0007.

Jaeger, J.C., and Cook, N.G.W. 1979. *Fundamentals of Rock Mechanics*. Third Edition. New York, New York: Chapman and Hall.

Popov, E.P. 1968. *Introduction to Mechanics of Solids*. Civil Engineering and Engineering Mechanics Series. Englewood Cliffs, New Jersey: Prentice-Hall.

SNL (Sandia National Laboratories) 2007. *Mechanical Assessment of Degraded Waste Packages and Drip Shields Subject to Vibratory Ground Motion*. MDL-WIS-AC-000001 REV 00. Las Vegas, Nevada: Sandia National Laboratories. ACC: DOC.20070917.0006; DOC.20080623.0002; DOC.20081021.0001.

RAI Volume 3, Chapter 2.2.1.3.2, Number 9:

Quantify the impact of localized corrosion on the drip shield legs on the drip shield vertical load-carrying capacity.

Basis: The screening argument for FEP 2.1.03.03.0B (SNL, 2008) indicates that localized corrosion could potentially initiate on the side support framework made of Titanium Grade 29, leading to plastic buckling of the sidewall.

1. RESPONSE

The structural response of the drip shield to severe localized corrosion has been approximated by a series of fully dynamic, two-dimensional, coupled rockfall/drip shield calculations that were performed to simulate the time-dependent interaction of the drip shield, waste package, and pallet within a rubble-filled drift (SAR Section 2.3.4.5.3.3.3). Calculations with a 10-mm thickness reduction for all drip shield components provide an approximation of drip shield response with severe localized corrosion on the sidewalls of the drip shield because the sidewalls are the thinnest and weakest structural components of the degraded drip shield, and because all of the external support beams and plates on the sidewalls of the drip shield are degraded with a 10-mm thickness reduction. Severe localized corrosion refers to the condition in which all the external support beams on the sidewalls of the drip shield are degraded by localized corrosion.

The results from the dynamic calculations show drip shield failure from buckling of the sidewalls, but the crown remains intact (i.e., retains its shape) for the most intense seismic ground motions at the 2.44 m/s and 4.07 m/s peak ground velocity (PGV) levels. Localized corrosion might also cause separation between adjacent drip shield, but a detailed evaluation of drip shield failure modes with localized corrosion indicates that axial separation of adjacent drip shields does not occur and that vertical separation of adjacent drip shields is limited and does not compromise the ability of the drip shield to deflect seepage and rockfall away from the waste package. The conclusion from these evaluations is that the drip shield retains its functionality to divert seepage and rockfall away from the waste package if localized corrosion severely degrades the Titanium Grade 29 support beams on the external sidewalls of the drip shield during the first 10,000 years after repository closure. This conclusion is consistent with FEP 2.1.03.03.0B (SNL 2008a), which excluded localized corrosion of the drip shield based on low consequence.

The response to this RAI evaluates: (1) the condition of the drip shield components and rockfall accumulation during the first 10,000 years after repository closure, (2) the drip shield/rockfall calculations that approximate drip shield response if localized corrosion occurs, and (3) the potential for axial or vertical separation between adjacent drip shields due to localized corrosion on the drip shield sidewalls. The impact of localized corrosion on excluded FEPs 2.1.07.05.0B, Creep of Metallic Materials in the Drip Shield; 2.1.03.03.0B, Localized Corrosion of Drip Shields; 2.1.06.05.0B, Mechanical Degradation of Invert; and 2.1.07.06.0A, Floor Buckling, is also considered here. Figure 1 is a simplified isometric that identifies the major components of the drip shield.

COMPONENT NAME	MATERIAL	MASS	QTY REQ
DS PLATE-1	SB-265 R52400	-	1
DS PLATE-2	SB-265 R52400	-	2
BASE	SB-575 N06022	-	2
STABILIZATION PIN ASSEMBLY	SB-575 N06022	-	10
BULKHEAD	SB-265 R56404	-	4
PERIPHERAL BULKHEAD	SB-265 R56404	-	2
BULKHEAD LONGITUDINAL STIFFENER	SB-265 R56404	-	15
INTERNAL SUPPORT PLATE	SB-265 R52400	-	10
EXTERNAL SUPPORT PLATE	SB-265 R52400	-	10
BULKHEAD FLANGE	SB-265 R56404	-	8
RIGHT SUPPORT BEAM-CONNECTOR	SB-265 R56404	-	2
LEFT SUPPORT BEAM-CONNECTOR	SB-265 R56404	-	2
SUPPORT BEAM-LARGE	SB-265 R56404	-	8
LIFTING FEATURE ASSEMBLY	SB-265 R56404	-	4
DS CONNECTOR GUIDE	SB-265 R52400	-	2
DSC PLATE-1	SB-265 R52400	-	1
DSC PLATE-2	SB-265 R52400	-	2
DSC CONNECTOR GUIDE	SB-265 R52400	-	2
DSC LEFT SUPPORT BEAM	SB-265 R56404	-	1
DSC RIGHT SUPPORT BEAM	SB-265 R56404	-	1
INTERLOCKING DRIP SHIELD	-	11,000 LBM 5,000 KG	-

02751DC_065.ai

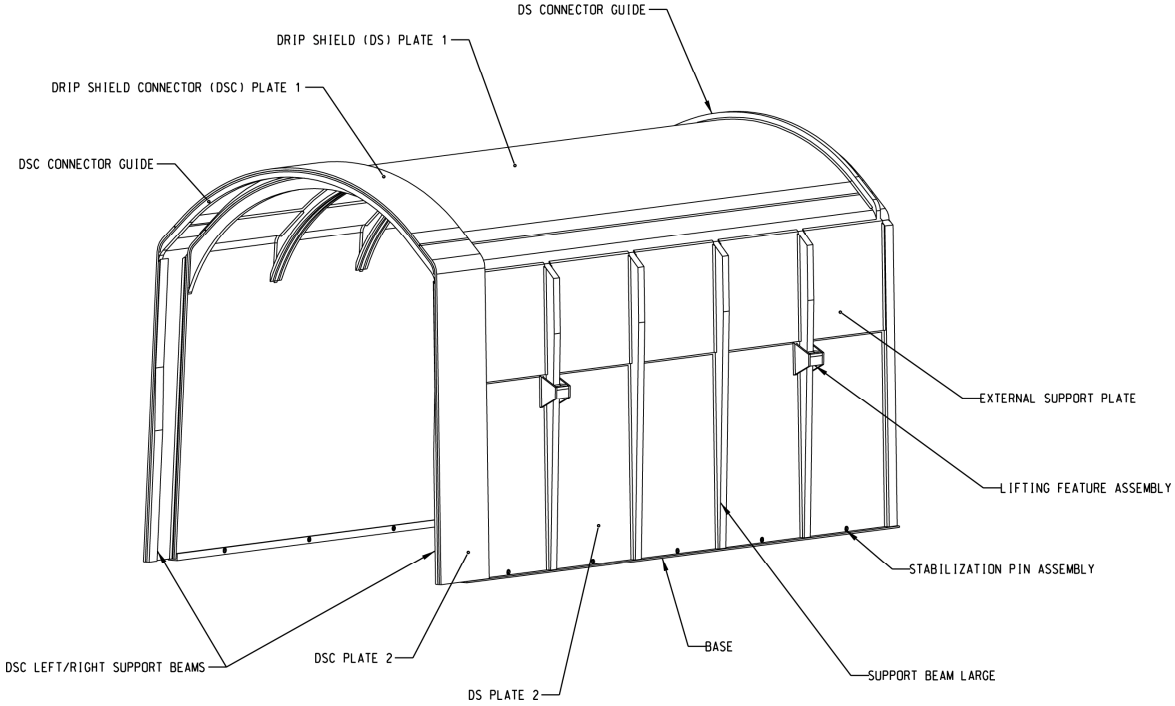

NOTE: DS = drip shield; DSC = drip shield connector (plate).

Figure 1. Simplified Isometric of the Drip Shield

1.1 IN-DRIFT CONDITIONS

1.1.1 Response of the Drip Shield to Localized Corrosion

Localized corrosion of drip shields composed of Titanium Grade 7 (SB-265 R52400) and Titanium Grade 29 (SB-265 R56404) has been excluded from TSPA on the basis of low consequence (SNL 2008a, excluded FEP 2.1.03.03.0B, Localized Corrosion of Drip Shields). According to the exclusion justification, localized corrosion of Titanium Grade 7 is not expected to initiate under repository-relevant conditions. Drip shield components fabricated from Titanium Grade 29 may be potentially susceptible to localized corrosion if they are directly exposed to seepage and to a subset of repository environments with unexpectedly aggressive chemical environments, although the effect of localized corrosion on the drip shield is predicted to have low consequence for TSPA (SNL 2008a, FEP 2.1.03.03.0B).

Localized corrosion requires an aqueous medium and is a function of pH, temperature, and the concentration of chloride ions in the seepage water, among other possible factors (SNL 2008a, FEP 2.1.03.03.0B). Localized corrosion is most likely to initiate when the maximum values for pH, temperature, and ionic concentrations occur during the rewetting period, directly after the thermal pulse, because the temperature of the aqueous medium will be greatest and because thermally driven evaporation and salt separation will increase the ionic concentrations relative to the post-10,000-year environment, when temperatures are cooler.

If localized corrosion occurs, it is likely to be intermittent spatially because of changing seepage and chemical environments throughout the repository. The large support beams on the external sidewalls of the drip shield are fabricated from Titanium Grade 29 (see Figure 1) and directly exposed to seepage, making these components potentially susceptible to localized corrosion in extreme chemical environments. If one or two of the support beams on a drip shield degrade as load-bearing components, the remaining support beams and the drip shield framework are expected to retain their structural integrity as a barrier to seepage and rockfall. Such a structurally degraded state can be approximated by a drip shield with both the structural members and plates thinned by 10 mm. This is a reasonable approximation because the lower sidewalls of the drip shield are among the thinnest structural components and because the sidewalls bear the full dynamic rockfall load and static dead weight of the drip shield. This response also considers the extreme case in which all the support beams of a drip shield become degraded as load-bearing components within a time scale that is very short relative to the 10,000-year time scale for FEP screening.

1.1.2 Response of the Drip Shield to General Corrosion

The drip shield plates, interior bulkheads, and longitudinal stiffeners remain essentially in their as-emplaced condition during the first 10,000 years after repository closure. These components are susceptible to general corrosion, but not localized corrosion, because localized corrosion is not expected to initiate under repository relevant conditions, because the plates are fabricated from Titanium Grade 7, which is not susceptible to localized corrosion (SNL 2008a, excluded FEP 2.1.03.03.0B), and because the interior bulkheads and longitudinal stiffeners are on the underside of the drip shield and therefore are not directly exposed to aqueous seepage.

The thickness reduction for the drip shield plates is estimated from the mean general corrosion rates for Titanium Grade 7 under benign conditions, 5.15 nm/yr (SNL 2007a, Table 8-1[a]), and under aggressive conditions, 46.1 nm/yr (SNL 2007a, Table 8-1[a]). Benign conditions are appropriate for the underside of the plates, without direct exposure to seepage, and aggressive conditions are appropriate for the top side of the plates, which have direct exposure to seepage. The mean, dual-sided thickness reduction of the plates over 10,000 years is estimated as: $(5.15 \times 10^{-9}$ m/yr + 46.1×10^{-9} m/yr)(10,000 years) = 5.125×10^{-4} m ~ 0.5 mm. This thickness reduction is negligible compared to the as-built thicknesses of the plates, which is 15 mm. Even a fourfold increase in the mean corrosion rates results in a thickness reduction of about 2 mm, which is still minor compared to the initial thickness of the plates.

The interior bulkheads and longitudinal stiffeners beneath the drip shield plates are fabricated from Titanium Grade 29. The general corrosion rate of Titanium Grade 29 is characterized as a cumulative distribution for the ratio of the Titanium Grade 29 rate to the sampled value of the general corrosion rate for Titanium Grade 7 (SNL 2007a, Section 6.2[a], fourth paragraph). The cumulative distribution is 1 up to the 50th percentile, 2.087 at the 86th percentile, and 6.679 at the 100th percentile (SNL 2007a, Table 6-8[a]). Using the maximum ratio of 6.679, the dual-sided thickness reduction for the interior bulkheads and longitudinal stiffeners beneath the plates is estimated as: (2)(6.679)(5.15×10^{-9} m/yr)(10,000 years) = 6.88×10^{-4} m ~ 0.7 mm. The general corrosion rate of 5.15×10^{-9} m/yr is appropriate here because these components are not directly exposed to the aggressive conditions on the top sides of the plates. This thickness reduction is negligible compared to the initial thickness of a bulkhead in its minimum dimension, 38-mm, and the initial thickness of a longitudinal stiffener in its minimum dimension, 38 mm. Even a fourfold increase in the corrosion rate under benign conditions results in a thickness reduction of less than 3 mm, which is minor compared to the initial thicknesses of a bulkhead or longitudinal stiffener.

It follows that the drip shield interior framework (bulkheads and stiffeners) and the drip shield plates remain essentially in their as-emplaced condition as structural elements during the first 10,000 years after repository closure.

1.1.3 Volume of Rockfall during 10,000 Years

Minimal rockfall accumulates in the repository during the first 10,000 years after repository closure. The mean rubble volume generated by seismic-induced rockfall is less than 5 m^3 per meter of drift length and 0.5 m^3 per meter of drift length for the lithophysal and nonlithophysal rock zones, respectively, for the first 10,000 years after repository closure (SAR Section 2.1, Figure 2.1-6). At 10,000 years, approximately 11% of realizations have lithophysal rockfall at or above 5 m^3 per meter of drift length, and approximately 1% of the realizations have lithophysal rockfall exceeding 60 m^3 per meter of drift length (SNL 2008b, Section 7.3.2.6.1.3.4). The curves for the 5th percentile and median are absent from SAR Figure 2.1-6 because a large number of realizations have very little or no drift degradation from seismic events during the first 10,000 years after repository closure.

These rubble volumes can be compared to the free volume on the sides of the drip shield to determine if the crown of the drip shield is covered with a significant amount of rubble. The diameter of the drift is 216 inches (SNL 2007b, Figure 6-107). The nominal widths of the drip shield at its base and shoulder are 99.8 inches and 89.48 inches, respectively. The average width is then (0.5)(99.8 + 89.48) = 94.64 inches. The shoulder height is 87.4 inches. The free area on the sides of the drip shield can be estimated as (216 inches – 94.64 inches)(87.4 inches) = 10,607 in^2 = 73.7 ft^2 = 6.8 m^2, equivalent to 6.8 m^3 per meter of drift. It follows that, even 10,000 years after repository closure, many realizations will have only minor rubble accumulation around the base of the drip shield and that the mean lithophysal rubble volume, which is less than 5 m^3 per meter of drift, contacts the sides the drip shield but does not cover the crown of the drip shield. Only 11% of the realizations have rockfall that exceeds 5 m^3 per meter of drift and have the possibility of covering the top of the drip shield.

1.2 IMPACT OF LOCALIZED CORROSION ON VERTICAL LOAD-CARRYING CAPACITY

Structural response calculations need not be performed for a 10,000-year localized corrosion scenario with completely degraded support beams on the sidewalls of the drip shield and an uncorroded framework of bulkheads, plates, and longitudinal stiffeners because the structural response for a localized corrosion scenario can be approximated by a series of fully dynamic two-dimensional discontinuum calculations performed to simulate the time-dependent interaction of the drip shield, waste package, and pallet within a rubble-filled drift (SAR Section 2.3.4.5.3.3.3). The dynamic calculations investigated the general effects of rubble loading on drip shield failure modes. The dynamic calculations focused on the 2.44 m/s and 4.07 m/s peak ground velocity (PGV) levels to investigate drip shield response during ground motions characteristic of the most intense seismic events. The ground motion time histories were selected to provide the maximum vertical components of peak ground acceleration (PGA) and PGV and the maximum total power spectral density for all three components. The ground motion time histories 3, 7, 9, and 13 were selected on this basis. Ground motion 9 has the largest vertical PGA, ground motions 7 and 3 have the largest vertical PGV values, and ground motion 13 has the largest power spectral density (the greatest energy content).

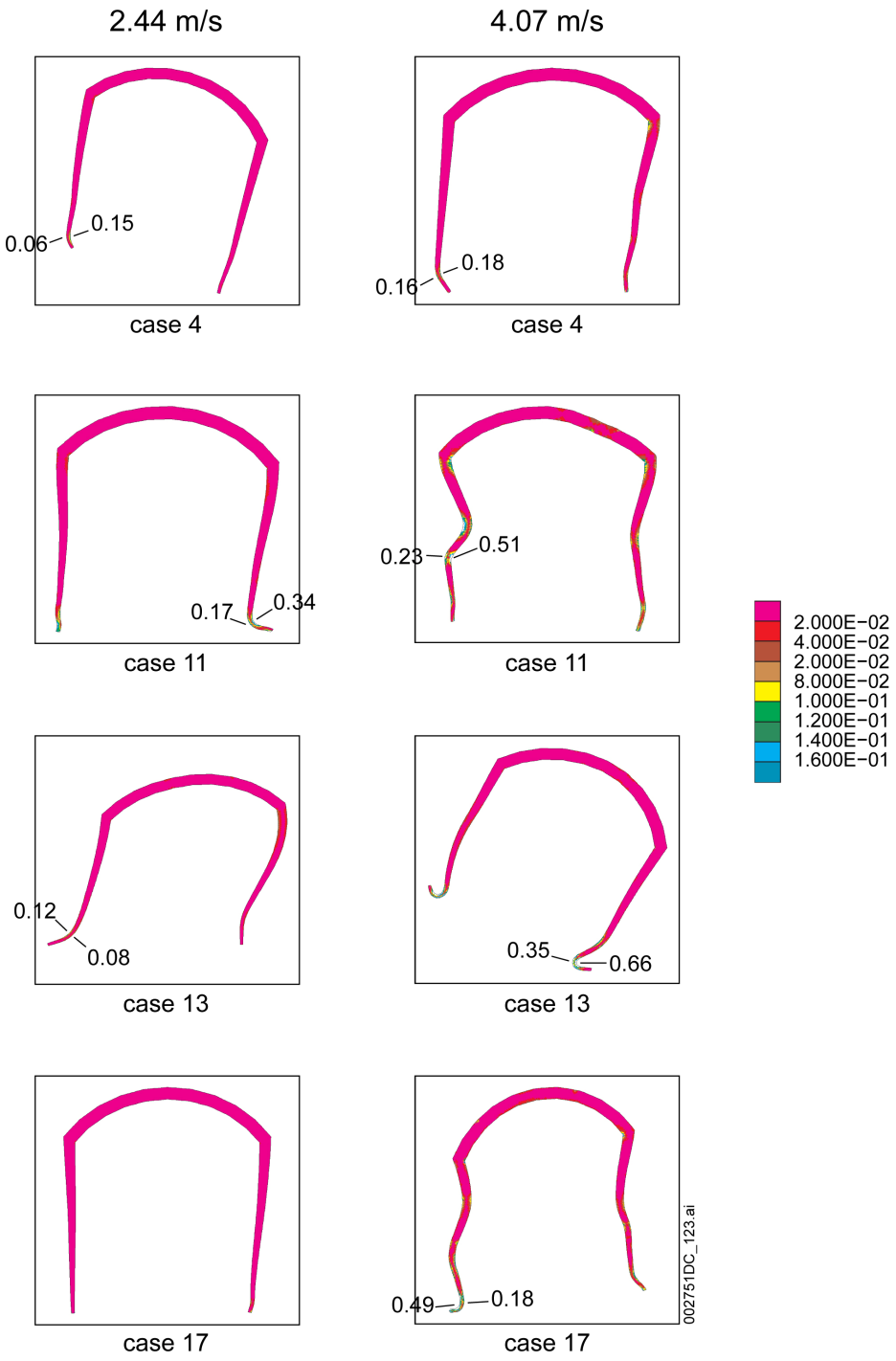

Source: SNL 2007c, Figure 6-62.

NOTE: Deformation is shown at true scale. The maximum effective plastic strain (obtained by multiplying the plastic shear strain by $\sqrt{4/3}$) is indicated in several cases where large distortion occurred.

Figure 2. Deformed Drip Shield Geometries and Contours of Plastic Shear Strain (Unitless) for All Drip Shield Components Uniformly Thinned by 10 mm

The fully dynamic calculations represent general corrosion of all drip shield components, rather than localized corrosion of the support beams. In this situation, the dynamic calculations with a 10-mm thickness reduction for all components are most representative for severe localized corrosion because all the large support beams on the sidewalls are highly degraded as load-bearing components. These calculations maximize the structural deformation of the crown of the drip shield relative to a localized corrosion scenario because the thicknesses of the crown components (plates, interior bulkheads, and longitudinal stiffeners) are reduced by 10 mm for the calculations, while the crown components are expected to remain essentially in their as-emplaced configuration during the first 10,000 years after repository closure (see Section 1.1.2 in this response). These calculations also maximize the structural deformation of the crown because the calculations are based on a fully collapsed drift, while the accumulated rockfall volume during the first 10,000 years after repository closure generally does not cover the top of the drip shield (see Section 1.1.3 of this response).

The computational results for eight dynamic cases (four ground motions at each of two PGV levels) are shown in Figure 2. Most of the eight cases show that a buckling failure mode is driving the deformation of the sidewalls of the drip shield. The crown is clearly intact (i.e., retains its shape) for these eight cases, which represent the most intense seismic events considered for the ground motion modeling case in the seismic scenario class, and the drip shield continues to surround the waste package even though the sidewalls show severe deformations. It follows that an uncorroded crown, as would occur with the localized corrosion scenario, will also retain its shape, surround the waste package, and continue to divert seepage and rockfall away from the drip shield even for the most intense seismic events.

1.3 POTENTIAL FOR DRIP SHIELD SEPARATION

Drip shield separation is defined as an axial gap or space between two adjacent drip shields that allows in-drift seepage to flow directly onto a waste package. Separation must be considered because it negates the functionality of the drip shield as a barrier to seepage and rockfall for the waste package. Separation could occur during a strong seismic ground motion event because of high plastic deformation in the drip shield's connector subassemblies or because of large relative vertical displacements between adjacent drip shields, all of which could be made possible by a degradation of the drip shield legs.

The potential for a seismic event to cause axial or vertical separation of adjacent drip shields in the absence of localized corrosion has been excluded from TSPA (SAR Sections 2.3.4.5.1.2 and 2.3.4.5.2.1.3.1; SNL 2008a, excluded FEP 1.2.03.02.0B, Seismic-Induced Rockfall Damages EBS Components) because: (1) ground motion amplitudes that are sufficient to cause separation are also large enough to partially or completely collapse drifts in the repository, (2) rockfall occurs within the first second or two of the arrival of these large amplitude ground motions, and (3) a kinematic study indicates that small static loads from rubble or frictional loads between EBS components are sufficient to prevent separation of drip shields. The technical details are provided in *Features, Events, and Processes for the Total System Performance Assessment: Analyses* (SNL 2008a) and in *Seismic Consequence Abstraction* (SNL 2007b Section 6.7.3).

The potential for localized corrosion of the external support beams to cause axial or vertical separation of adjacent drip shields is the focus of this discussion, which considers three failure modes for the drip shield: (1) the drip shield fails from its own dead weight; (2) the drip shield fails during a low intensity seismic event with a PGV level less than 1 m/s; and (3) the drip shield fails during a high intensity seismic event with a PGV level greater 1 m/s.

Failure mode (2) will generally have some lithophysal rockfall that at least partly fills the sides of the drip shield, based on the discussion of rockfall volumes in Section 1.1.3 and based on the typical rockfall from a seismic event with a PGV level less than 1 m/s (SNL 2007b, mean rockfall volumes in Figure 6-56). For example, the mean lithophysal rockfall volume is 7.8 m^3 per meter of emplacement drift at the 1.05 m/s PGV level (SNL 2007b, Table 6-32). Failure mode (3) will have lithophysal rockfall that partly or fully covers the crown of the drip shield because more intense seismic events generate a large volume of lithophysal rockfall, as shown in (SNL 2007b, Figure 6-57). For example, the mean lithophysal rockfall volume is 86.9 m^3 per meter of emplacement drift at the 2.44 m/s PGV level (SNL 2007b, Table 6-32). The presence of even minimal rockfall eliminates the potential for drip shield separation, as discussed in (SNL 2007b Section 6.7.3), so failure modes (2) and (3) are eliminated as a cause of drip shield separation.

Rockfall volumes in the nonlithophysal units are substantially less than in the lithophysal units (SNL 2007b, Section 6.7.2.1). The mean nonlithophysal rockfall volumes at the 1.05 m/s and 2.44 m/s PGV levels are 0.24 m^3 per meter of drift and 0.46 m^3 per meter of drift, respectively (SNL 2007b, Table 6-32). Minimal levels of rockfall will help to eliminate the potential for drip shield separation, as discussed in *Seismic Consequence Abstraction* (SNL 2007b, Section 6.7.3). If no rockfall occurs in the nonlithophysal units, the analysis for failure mode (1) is applicable.

Failure mode (1), which is failure from the static weight of the drip shield, could result in vertical separation between adjacent drip shields if localized corrosion occurs on all the large support beams of a single drip shield and if the neighboring drip shields do not experience localized corrosion. In this case, the sidewalls of the single drip shield with localized corrosion can buckle, with a resulting vertical displacement relative to its adjacent neighbors. However, significant vertical displacement can only occur on one end of the drip shield because the drip shield connector plate (DSC plate) on the failed drip shield overlaps its adjacent neighbor, which will provide structural support for one end of the failed drip shield. The other end of the failed drip shield, opposite the DSC plate, could move vertically until it rests on the waste package beneath the drip shield, resulting in a vertical separation.

The magnitude of the vertical separation can be estimated by the vertical clearance between the top of a waste package and the underside of the drip shield, which varies between 14 inches and 27 inches (SNL 2007b, Figure 6-107). These vertical displacements are small enough that the interlocking mechanism holding adjacent drip shields together is still engaged and functional, so axial separation is not a concern for failure mode (1).

The DSC plate on the adjacent, unfiled drip shield is 320 mm wide in the longitudinal direction, overlaps the adjacent, failed drip shield at the location of the vertical separation, and will retain its shape because the crown remains essentially uncorroded over 10,000 years (see Section 1.1.2). The DSC plate will therefore deflect seepage and rockfall that falls in the vertical plane of the separation away from the waste package.

Seepage could also fall on the body of the failed drip shield, away from the plane of separation. Seepage is expected to be shed laterally, flowing directly down the sides of the drip shield, because the crown retains its curved shape after the sidewalls buckle. In the event that seepage flows longitudinally toward the vertical separation, a drip shield connector guide is located on the top surface of the lower end of the failed drip shield and will deflect seepage down the sides of the drip shield before it drips onto the waste package. The drip shield connector guide is fabricated from Titanium Grade 7 (see table in Figure 1), has a square cross-section, 1.97-inch by 1.97-inch, is not susceptible to localized corrosion, and is highly resistant to generalized corrosion.

An alternate scenario for failure mode (1) is that all the drip shields in an emplacement drift experience localized corrosion and fail by buckling of the sidewalls to one degree or another. Each drip shield is mechanically connected to one adjacent neighbor because its DSC plate overlaps the adjacent neighbor. This overlap will spread the loads among all the drip shields, leading to a more uniform response, although some vertical separations would still be expected to occur. The DSC plate is expected to retain its shape because the crown remains essentially in its as-emplaced configuration over 10,000 years. The DSC plates will therefore deflect seepage and rockfall that falls in the vertical plane of the separation away from the waste package. The drip shield connector guides will also remain in their as-emplaced configuration, deflecting any seepage that flows longitudinally toward the vertical separation down the sides of the drip shield before it drips onto the waste package. Axial separation is not expected to occur because the maximum vertical displacements, which are limited by the presence of the waste package and pallets, are small enough that the interlocking mechanism holding adjacent drip shields together is still engaged, so axial separation is not a concern for failure mode (1).

In summary, failure mode (1) will not cause axial separation between adjacent drip shields but may cause vertical separation between adjacent drip shields; however, the presence of the DSC plate and the drip shield connector guide prevent seepage from dripping onto a waste package. Failure modes (2) and (3) will not cause axial or vertical drip shield separation because the presence of even minimal rockfall eliminates the potential for drip shield separation, as discussed in *Seismic Consequence Abstraction* (SNL 2007b, Section 6.7.3).

The drip shield design is controlled such that a series of interlocked drip shields resist separation through failure of the drip shield connector guides, the drip shield connector left-right support beams, and the left-right support beam connectors, or through failure of the welds holding these drip shield components in place during a seismic event (SAR Table 1.9-9, Design Control Parameter 07-08). This design constraint provides a margin of safety against separation.

1.4 CONSISTENCY WITH RELATED FEPS

This RAI response supports the conclusions in FEP 2.1.03.03.0B, Localized Corrosion of Drip Shields, that the drip shield continues to function as a barrier to seepage and rockfall during the first 10,000 years after repository closure.

Localized corrosion of the external support beams of the drip shield has no relevance to excluded FEP 2.1.07.05.0B, Creep of Metallic Materials in the Drip Shield, because once localized corrosion occurs it is assumed to degrade the large support beams instantaneously relative to the 10,000-year time scale for FEP screening, leading to sidewall buckling on a much shorter time scale than creep-related processes. Excluded FEPs 2.1.06.05.0B, Mechanical Degradation of Invert, and 2.1.07.06.0A, Floor Buckling, are not relevant for this analysis because it is assumed that the sidewalls buckle once localized corrosion is initiated, independent of the condition of the floor and invert.

1.5 CONCLUSIONS

The structural response of the drip shield to the potential impacts of severe localized corrosion has been approximated by a series of fully dynamic two-dimensional discontinuum calculations that were performed to simulate the time-dependent interaction of the drip shield, waste package, and pallet within a rubble-filled drift (SAR Section 2.3.4.5.3.3.3). The computational results show inelastic deformation of the sidewalls of the drip shield, but the crown remains intact (i.e., retains its shape) for the most intense seismic ground motions at the 2.44 m/s and 4.07 m/s PGV levels. Analysis of the potential for drip shield separation due to sidewall buckling also indicates that the drip shield will retain its ability to deflect seepage and rockfall away from the waste package if localized corrosion degrades all of the Titanium Grade 29 support beams on the sidewalls of the drip shield.

2. COMMITMENTS TO NRC

None.

3. DESCRIPTION OF PROPOSED LA CHANGE

None.

4. REFERENCES

SNL 2007a. *General Corrosion and Localized Corrosion of the Drip Shield*. ANL-EBS-MD-000004 REV 02 ADD 01. Las Vegas, Nevada: Sandia National Laboratories. ACC: DOC.20070807.0004.

SNL 2007b. *Seismic Consequence Abstraction.* MDL-WIS-PA-000003 REV 03. Las Vegas, Nevada: Sandia National Laboratories. ACC: DOC.20070928.0011.

SNL 2007c. *Mechanical Assessment of Degraded Waste Packages and Drip Shields Subject to Vibratory Ground Motion*. MDL-WIS-AC-000001 REV 00. Las Vegas, Nevada: Sandia National Laboratories. ACC: DOC.20070917.0006.

SNL 2008a. *Features, Events, and Processes for the Total System Performance Assessment: Analyses*. ANL-WIS-MD-000027 REV 00 ACN 01. Las Vegas, Nevada: Sandia National Laboratories. ACC: DOC.20080307.0003; DOC.20080407.0009.

SNL 2008b. *Total System Performance Assessment Model-Analysis for the License Application*. MDL-WIS-PA-000005 REV 00. Las Vegas, Nevada: Sandia National Laboratories. ACC: DOC.20080312.0001.